Macromolecules

Nonlinear Shear Rheology of Entangled Polymer Rings

Daniele Parisi, Salvatore Costanzo, Youncheol Jeong, Junyoung Ahn, Taihyun Chang, Dimitris Vlassopoulos,* Jonathan D. Halverson, Kurt Kremer, Ting Ge, Michael Rubinstein,* Gary S. Grest, Watee Srinin, and Alexander Y. Grosberg*

Read Online

ACCESS | 📊 Metrics & More | 📰 Article Recommendations | 🆂🅸 Supporting Information
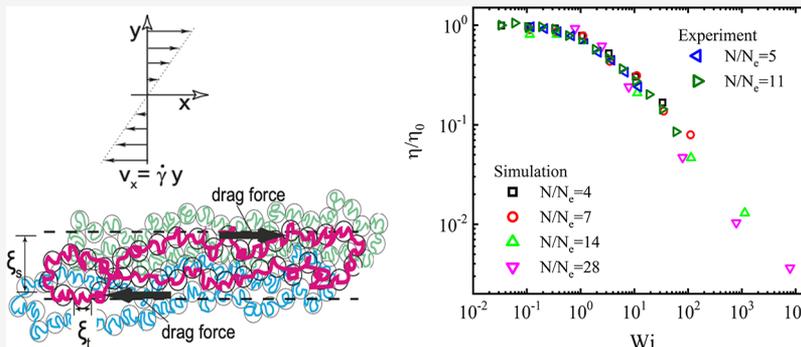
ABSTRACT: Steady-state shear viscosity $\eta(\dot{\gamma})$ of unconcatenated ring polymer melts as a function of the shear rate $\dot{\gamma}$ is studied by a combination of experiments, simulations, and theory. Experiments using polystyrenes with $Z \approx 5$ and $Z \approx 11$ entanglements indicate weaker shear thinning for rings compared to linear polymers exhibiting power law scaling of shear viscosity $\eta \sim \dot{\gamma}^{-0.56 \pm 0.02}$, independent of chain length, for Weissenberg numbers up to about 10^2. Nonequilibrium molecular dynamics simulations using the bead-spring model reveal a similar behavior with $\eta \sim \dot{\gamma}^{-0.57 \pm 0.08}$ for $4 \leq Z \leq 57$. Viscosity decreases with chain length for high $\dot{\gamma}$. In our experiments, we see the onset of this regime, and in simulations, which we extended to $Wi \sim 10^4$, the nonuniversality is fully developed. In addition to a naive scaling theory yielding for the universal regime $\eta \sim \dot{\gamma}^{-0.57}$, we developed a novel shear slit model explaining many details of observed conformations and dynamics as well as the chain length-dependent behavior of viscosity at large $\dot{\gamma}$. The signature feature of the model is the presence of two distinct length scales: the size of tension blobs and much larger thickness of a shear slit in which rings are self-consistently confined in the velocity gradient direction and which is dictated by the size of a chain section with relaxation time $1/\dot{\gamma}$. These two length scales control the two normal stress differences. In this model, the chain length-dependent onset of nonuniversal behavior is set by tension blobs becoming as small as about one Kuhn segment. This model explains the approximate applicability of the Cox−Merz rule for ring polymers.

■ INTRODUCTION

Understanding polymer rheology is important to the processing and fabrication of polymeric materials. Linear rheology of both unentangled and entangled solutions and melts of linear chains has been mostly understood[1] based on various molecular models, such as the Rouse, Zimm, and tube models for dynamics in different regimes.[2] Among polymers with other architectures, the case of branched polymers such as stars was also examined (e.g., ref 3; see also books[1] (section 7.10) and[2] (section 9.4.2)).

Rheology of ring polymers has attracted attention much more recently, not only because ring polymers are promising as materials but also from the physics point of view since rheology of long linear polymers is controlled by reptation, which is fundamentally dependent on chain ends, and as rings have no ends, they must behave very differently (see, e.g., ref 4. In fact, long unconcatenated rings are very different from linear

chains even in thermodynamic equilibrium. In particular, rings in the melt of other long rings adopt a compact state with gyration radius scaling as $N^{1/3}$ as a function of the number of monomers N compared to $\sim N^{1/2}$ for linear chains.[5,6] Since rings are so dramatically different from ideal Gaussian due to topological uncrossability, a concentrated system of sufficiently long rings is called entangled, even though they are unconcatenated. To further contrast linear chains and rings, every segment in the entangled system of linear chains is surrounded and restricted almost exclusively by the segments

of other chains, while in an entangled ring system, motion of every segment is constrained by both inter- and intrachain interactions. In the rheological context, entangled, unconcatenated ring polymer melts behave very differently from their linear counterparts, even in the linear response regime, exhibiting a power law stress relaxation[7] $G(t) \sim t^{-\beta}$, with exponent $\beta \approx 0.4$ without the rubbery plateau characteristic of linear polymers,[1] as predicted by various models[7,9] and observed in both experiments[7] and simulations.[10] Various other aspects of ring polymers also attracted much attention recently (see, e.g., refs 6 and 11−19).

In contrast to the linear response regime, the nonlinear rheology of even linear polymers has been only partially understood and presents a significant challenge.[20] One prominent manifestation of nonlinear rheological behavior is that the viscosity η of a polymer solution or melt in steady shear crosses over from the shear rate-independent plateau to the shear thinning regime where η decreases with the increasing shear rate $\dot{\gamma}$. This behavior can be described by the expression[1]

$$\eta(\dot{\gamma}) = \frac{\eta_0}{(1 + \dot{\gamma}\tau_{\text{relax}})^\alpha} \tag{1}$$

where η_0 is the viscosity in the limit of the zero shear rate, τ_{relax} is the crossover time, which is usually the same as terminal relaxation time of the chain, and α is the shear thinning exponent (see, e.g., refs 21−25).

The nonlinear rheology of entangled, unconcatenated ring polymers only very recently started attracting attention. New advances in instrumentation have paved the way to obtain accurate experimental data in nonlinear shear and uniaxial extension.[26,27] In fact, experiments and simulations were reported in the last few years, showing fragmental evidence of low-extension rate thickening[26,28,29] and high-shear rate thinning;[27] see also earlier simulations by Halverson et al.,[30] simulations of rings in connection with interfacial behavior,[31] and a recent paper by Tsamopoulos et al.[32] Simulations of individual ring polymers in dilute solutions, accounting for finite extensibility and hydrodynamic effects, indicate the occurrence of shear thinning.[33−36] In this paper, we present systematic data of rheology experiments, molecular dynamics simulations, and theoretical scaling estimates to shed light on the shear rheology of highly entangled, unconcatenated ring polymers in the strongly nonlinear shear regime.

One way to look at nonlinear shear viscosity is to apply the empirical Cox−Merz rule,[37] which states that the steady shear viscosity $\eta(\dot{\gamma})$ at a given shear rate $\dot{\gamma}$ is (approximately) equal to the absolute value of complex viscosity $|\eta*(\omega)|$ at the frequency $\omega = \dot{\gamma}$. Given that in the linear response regime, entangled, unconcatenated rings exhibit self-similar power law relaxation with the modulus $G(t) \sim t^{-\beta}$ (see ref 7), the Cox−Merz rule predicts a universal shear thinning exponent $\alpha = 1 - \beta \approx 0.6$, which, as we shall show, agrees well with both experiments and simulations. For entangled linear polymers, the situation is more complex, as it involves tube deformation. Somewhat surprisingly, the Cox−Merz rule still can be made to work reasonably well, by approximating a rubbery plateau by a very weak exponent $\beta \approx 0.1-0.2$, which transfers into $\alpha = 1 - \beta \approx 0.8-0.9$, in agreement with our simulations and experiments.

While the Cox−Merz rule works in many cases, it sheds little light on the actual structure and dynamics of polymers in nonlinear shear flow, its applicability limits are not clear, and

its reliance on the absolute value of complex viscosity seems rather arbitrary from a theoretical standpoint, only justified empirically. Indeed, the dynamic viscosity $|\eta*(\omega)|$ corresponds to relaxed polymers, while these polymers are expected to be strongly deformed in nonlinear shear. To go beyond this purely empirical rule, we first apply the Rabin and Öttinger[38] idea of "shear blobs"—polymer sections of g_s monomers with relaxation time $\tau(g_s) = 1/\dot{\gamma}$. Assuming additionally that dissipation is dominated by the modes with relaxation times shorter than $1/\dot{\gamma}$, we formulate a new version of the Cox−Merz rule that not only reproduces the result $\alpha = 1 - \beta$ but lends missing molecular justification for the rule itself. Unfortunately, upon a closer look, this scaling theory proves to be somewhat naive in terms of its theoretical basis and not entirely satisfactory in terms of comparison with experiments and simulations. Indeed, why do longer wavelength modes not contribute to dissipation? Furthermore, since rings are expected to become strongly stretched (similar to other previously examined systems, such as linear DNA under a steady shear flow (visualized through fluorescence microscopy[39]), and observed in many computer simulations of linear chains[40−44]), it is tempting to imagine them developing some entropic elasticity, but how does it happen in a nonequilibrium system on the scale far above the shear blob size? At the same time, our molecular dynamics simulation data indicate that at a large shear rate $\dot{\gamma}$, shear thinning is no longer universal, it deviates from the power law (eq 1), and surprisingly, viscosity of longer chain melts becomes smaller than that of melts of shorter chains. Our experimental data also indicate the onset of this new regime at the largest shear rate $\dot{\gamma}$. These observations point to chain elongation along the flow direction as a likely key to improve naive scaling theory.

Thinking about chains in a shear field as elongated in the flow direction, Colby et al.[45] were the first to construct a scaling argument for unentangled melts of linear polymers based on tension blobs, the length scale above which chain sections are stretched by shear stress. These authors assumed that the array of tension blobs does not fluctuate in the transverse direction (unlike chains under tension), thus effectively identifying tension blobs with shear blobs, while in fact, there is no reason to believe that these two blob scales are the same.

Here, we suggest a novel hybrid "shear slit model" that combines tension blobs and shear blobs in one unified picture, shown schematically in Figure 1. The key idea is that the shear blob length scale, ξ_s, and the tension blob length scale, ξ_t, are qualitatively different because dynamics of modes is very different in the flow direction x and in the velocity gradient direction y. In the y direction, a chain is effectively dynamically confined in a slit of thickness on the order of shear blob size ξ_s while at the same time, it is strongly stretched in the x direction to such an extent that tension blob size ξ_t is smaller than the confinement scale: $\xi_t < \xi_s$. In this sense, the situation is reminiscent of a classical polymer physics problem where a chain, confined in the y direction into a slit, is also simultaneously strongly stretched in the x direction. The size of shear blobs and shear viscosity in this universal regime are independent of molecular weight, while tension blobs are smaller (and the magnitude of tension is larger) for longer chains. The nature of confinement by nonlinear shear flow is purely dynamical: if a section of one particular "test" chain (magenta in Figure 1) extends by fluctuation beyond the ξ_s scale, then it is typically turned (or advected) back by the
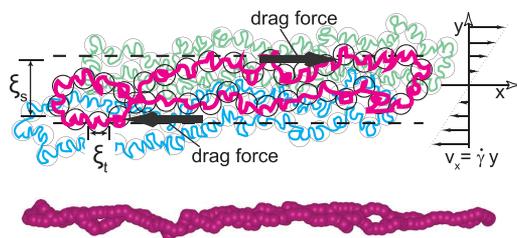
Figure 1. Schematic cartoon of the shear slit model. Each ring in a strong shear flow is dynamically self-consistently confined to a slit whose thickness in the velocity gradient direction is ξ_s, the size of a chain section with g_s monomers and relaxation time $\tau(g_s) = 1/\dot{\gamma}$. At the same time, the chain is strongly stretched in the flow velocity direction and can be viewed as an array of tension blobs of size $\xi_t < \xi_s$ with the number of monomers $g_t < g_s$. Notice that chains very strongly overlap. The lower image is a simulation snapshot taken for $N = 200$ and $Wi = 34$.

neighboring chains (blue and green in Figure 1) passing by the test chain. We assume that the relaxation time for longitudinal modes in the x direction is shorter than the typical time between episodes when the chain tumbles as a whole. Therefore, these modes equilibrate over distances larger than the shear blob size, thus generating entropic elastic response to stretching. At the same time, transverse modes in the y direction are effectively suppressed on length scales larger than ξ_s thus not contributing to viscosity. Indeed, dissipation is controlled by the interchain frictional contacts of sections of neighboring chains, while relative velocity in these contacts is limited to about $\xi_s\dot{\gamma}$ by confinement of every chain in the y direction. As we shall see, this limitation of relative speed sets the relation between tension and shear blobs, thus explaining shear thinning and giving a foundation to the Cox–Merz rule, in both our modified and the traditional formulations.

The two length scales of shear and tension blobs are intimately related to the two normal stress differences that can be directly measured in experiments or simulations. The nature of these blobs provides simple explanation for the opposite signs of the two normal stress differences and explains their dependence on the shear rate.

Our novel shear slit model provides natural explanation for the above mentioned counterintuitive observations of viscosities not only deviating from the law (eq 1) but getting smaller for long chains than for short ones. This happens because of the interplay between tension and shear blobs: when chain stretching in the flow direction becomes so strong that tension blobs become comparable to chain Kuhn segments, this stretching starts affecting shear blobs reducing their size in the flow gradient direction, thus reducing viscosity, and this mechanism works more efficiently for longer chains due to larger stretching force.

We develop a shear slit model specifically for rings because the case of rings is simpler, as their self-similar dynamics extends over a wider range of chain lengths. Indeed, self-similar Rouse dynamics for a melt of linear chains is characteristic only for the unentangled regime, at $N < N_e$, where N_e is the number of monomers per entanglement. Quantitatively, we follow the historical definition of N_e for linear chains as a dynamic property that can be determined for a particular polymer by a dynamic measurement in experiments or in simulation, such as, e.g., finding the plateau modulus. Dynamics of entangled linear chains is dominated by reptation, depends on chain ends, and is not self-similar. By contrast, both structure and dynamics of ring melts remain self-similar in the entangled regime at $N \gg N_e$, where N_e is the same parameter determined for linear polymers of the same nature[3].

This article is organized as follows. We first describe our experimental study of a melt of polystyrene rings. Then, we report the results of molecular dynamics simulations of ring polymers using a bead-spring model. In both experimental and computational studies, the rings are in the entangled regime (up to $Z = N/N_e = 11$ in experiments and $Z = 57$ in simulations) for the Weissenberg number Wi, based on terminal relaxation time, on the order of 10^2 in experiments and 10^4 in simulations. For both experiments and simulations, we present for comparison original data for nonlinear rheology of entangled linear chains. Then, we describe naive scaling theory based on shear blobs, introduce the shear slit model, and conclude by reviewing the remaining open questions.
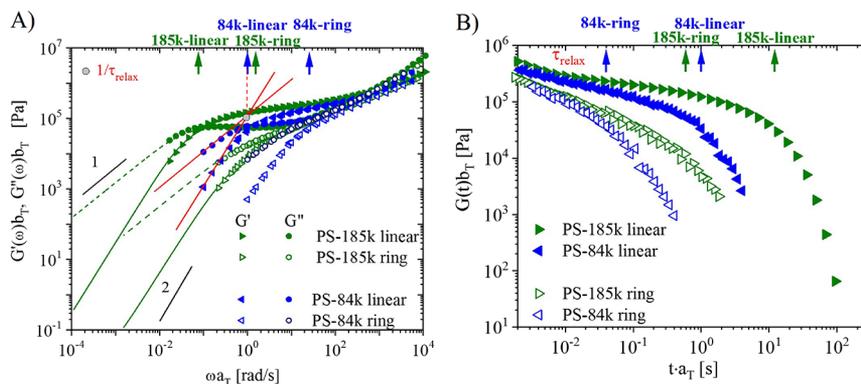
Figure 2. (A) Linear viscoelasticity frequency-dependent storage (triangles) and loss (circles) moduli and (B) time-dependent stress relaxation moduli of ring (open symbols) and linear (filled symbols) PS, 84k (blue) and 185k (green) at the reference temperature $T_{ref} = 150$ °C. Solid and dashed green lines have been obtained by means of creep experiments converted into dynamic moduli. A creep experiment consists of applying a constant stress, small enough to ensure linear viscoelasticity, for a given time. The creep compliance is then followed over time until the system reaches the flow regime, allowing it to extend the data into the low-frequency region. Red lines (shown only for the example of PS-84k linear) illustrate the graphic procedure of determining terminal relaxation frequency by finding the intersection of low-frequency limiting power laws of $G'(\omega) \sim \omega^2$ and $G''(\omega) \sim \omega$. Resulting frequencies ω_{relax} are shown by arrows for all four samples in figure A, and corresponding relaxation times $\tau_{relax} = 1/\omega_{relax}$ are shown in figure B.

■ EXPERIMENTS

Materials and Experimental Methods. Polystyrene (PS) ring samples were synthesized by ring closure of telechelic polystyrene, which was prepared in THF by anionic polymerization using potassium naphthalenide as an initiator. The used samples are nearly monodisperse (their polydispersity based on size-exclusion chromatography does not exceed a value of 1.01, see the Supporting Information). Additional details about synthesis, purification, and characterization schemes are described elsewhere.[48,49] Ring polymers are very sensitive to linear contamination. A tiny amount of a linear component added to ring systems will induce a dramatic change in their rheological behavior. Unfortunately, conventional liquid chromatography cannot effectively purify the ring sample. Here, the ring samples are purified by LCCC (liquid chromatography at critical condition) fractionation, the technique that can effectively purify the ring samples, making the residual linear contamination hardly detectable by any analysis. Although some amount of linear chains below the detection threshold perhaps remains in our sample, its insignificance is further confirmed by the agreement (see below) of our experimental data with simulations, which are certainly linear-free. Further details regarding ring synthesis and fractionation are relegated to the Supporting Information.

Rheological measurements were performed on a strain-controlled ARES rheometer (TA Instruments, USA), equipped with a force rebalance transducer (2KFRTN1). In order to avoid artifacts due to edge fracture, a homemade cone partitioned-plate (CPP) fixture was used. Details can be found in references[27,50] and more complete discussion in ref 51; see also the Supporting Information.

Experimental Results. *Linear Viscoelasticity.* Figure 2 compares the linear viscoelastic properties for PS-84k and PS-185k ring and linear polystyrene at a reference temperature of T_{ref} = 150 °C. Figure 2A shows frequency-dependent storage $G'(\omega)$ and loss $G''(\omega)$ moduli, while Figure 2B shows time-dependent relaxation moduli $G(t)$; they are Fourier-transformed master curves of the frequency-dependent storage and loss moduli.

Storage and loss moduli were obtained by means of small amplitude oscillatory shear measurements at different temperatures and application of the time−temperature superposition principle (which involves shifting the data obtained at different temperatures with respect to T_{ref} = 150 °C). The horizontal shift factors for the frequency follow the empirical Williams−Landel−Ferry equation (see, e.g., ref 52) log $a_T = -C_1(T - T_{ref})/(C_2 + T - T_{ref})$, where the constants C_1 = 7.2 and C_2 = 103 K were obtained from the fit of this equation to the data.[27,50] The vertical shift factors $b_T = \rho(T)T/\rho(T_{ref})T_{ref}$ for the moduli reflect the temperature−density compensation. The temperature dependence of the density (in g/cm^3) is[53] $\rho(T)$ = 1.2503 − 6.05 × 10^{-4}T, where T is the absolute temperature (in K).

Fitting $G(t)$ to exp$(-t/\tau_{relax})$ at long times for every chain length and architecture, or, equivalently, finding the intersection of low-frequency limiting power laws of $G'(\omega) \sim \omega^2$ and $G''(\omega) \sim \omega$ (auxiliary red lines in Figure 2A), we find the terminal time and terminal frequency $\omega_{relax} = 1/\tau_{relax}$. Through this procedure, we found that at reference temperature T_{ref} = 150 °C for linear PS-84k and PS-185k, τ_{relax} = 1.0 and 12.8 s, respectively, and for rings PS-84k and PS-185k, τ_{relax} = 0.040 and 0.60 s (all indicated by arrows in both panels of Figure 2; see refs 26 and 27 for further details about slow modes).

Nonlinear Rheology. Figure 3 reports the steady-state viscosity (obtained from transient measurements at discrete shear rates) as a function of the shear rate, $\eta(\dot{\gamma})$, for rings PS-185k and PS-84k, along with the respective linear precursors, at the same temperature of 150 °C. The value of η at each rate was obtained as an average over the final steady-state portion of the start-up curves. The standard deviation was negligible (error bars smaller than the size of the symbols). At low shear rates, the data of different samples (with the exception of PS-185k linear) tend toward the zero shear limiting viscosities, which strongly depend on molar mass and macromolecular structure. Within the range of shear rates tested in our experiments, the viscosities of different samples approach each other with increasing $\dot{\gamma}$, consistent with expectations from the Cox−Merz rule.
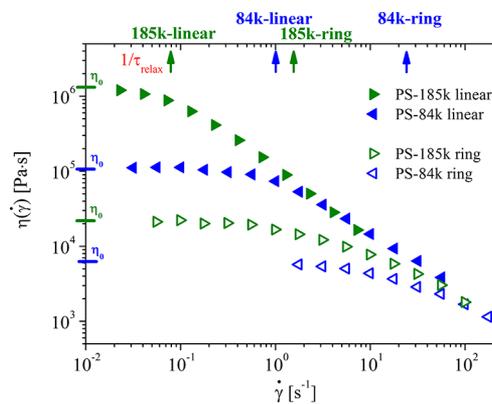
Figure 3. Steady viscosity versus shear rate for ring (open triangles) and linear (filled triangles) PS, 84k (left-pointing triangles) and 185k (right-pointing triangles). Limiting values of viscosity at $\dot{\gamma} \to 0$ are indicated on the vertical axis. The reference temperature is 150 °C. The values of shear viscosity presented in this plot are given in the Supporting Information, Table S2.

Nevertheless, linear and ring polymers exhibit different shear thinning slopes as discussed below.

A closer look at Figure 3 suggests that viscosity of the longer rings drops down at a faster rate than for shorter rings, and they nearly coincide at the highest reported $\dot{\gamma}$. In fact, it is our theoretical prediction, also consistent with simulation findings (see below) that these curves first merge in the universal regime, with shear viscosity independent of molecular weight, and then, they drop below the universal curve, with higher-molecular-weight polymers dropping earlier and lower-molecular-weight polymers later, at higher shear rates; in other words, beyond the universal regime, at large $\dot{\gamma}$, viscosity becomes a decreasing function of the chain length.

Knowing (from separate measurements) the terminal relaxation times τ_{relax} for all our samples (see above), we can replot the steady-state shear viscosities, normalized by their respective zero shear values, as functions of the Weissenberg number $Wi = \dot{\gamma}\tau_{relax}$ data (see Figure 4). Note that the determination of τ_{relax} is the main source of horizontal errors in Wi and hence error bars in Figure 4. To check applicability of the Cox−Merz rule, we present in the same figure the absolute values of respective complex viscosities[4] normalized by their zero frequency values as functions of the Deborah number, $De = \omega\tau_{relax}$ (a good explanation about Weissenberg and Deborah numbers can be found in ref 54). By definition, normalized complex and shear viscosities should reach a value of 1 for $De \ll 1$ and $Wi \ll 1$. The nonlinear data for shear viscosity $\eta(\dot{\gamma})$ overlap with the linear data for the absolute value of complex viscosity $|\eta^*(\omega)|$ reasonably well at $Wi \lesssim 30$ within experimental error, complying with the Cox−Merz rule, for both linear and ring polymers. At higher shear rates, the nonlinear data are systematically lower than the linear ones, which indicates stronger shear thinning. This effect, at least for the rings, is consistent with the theoretical shear slit model, proposed below (because the size of the shear blob becomes smaller due to partial orientation of Kuhn segments, leading to stronger shear thinning). At these high shear rates, our experiments approach the limit where we cannot rule out some experimental artifacts, despite precautions taken, related possibly to onset of weak wall slip or edge fracture propagating up to the gap between the partition and cone of the CPP.

■ SIMULATIONS

Simulation Methods. The bead-spring model[55] is used in the molecular dynamics (MD) simulations. Each polymer contains N spherical beads of size σ and mass m. Beads interact via the truncated and shifted Lennard-Jones potential with interaction strength ε cutoff at $r_c = 2^{1/6}\sigma$. All quantities in the simulations are expressed in terms of σ, ε, and the characteristic time $\tau_{LJ} = \sigma(m/\varepsilon)^{1/2}$. Neighboring beads in a
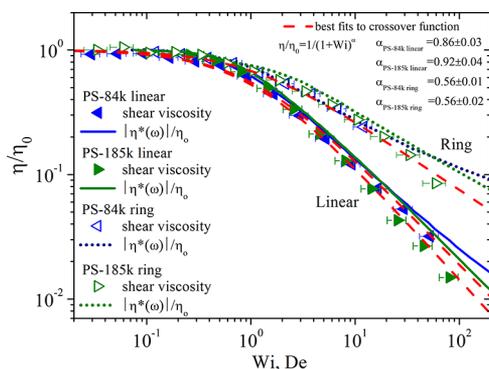
Figure 4. Steady shear viscosity (obtained from steady shear measurements, triangles), normalized by zero shear viscosity η_0, as a function of the Weissenberg number $Wi = \dot{\gamma}\tau_{\text{relax}}$ and the absolute value of complex viscosity $|\eta^*(\omega)| = \sqrt{G'(\omega)^2 + G''(\omega)^2}/\omega$ (solid or dotted lines), also normalized by η_0, as a function of the Deborah number $De = \omega\tau_{\text{relax}}$. In both cases, τ_{relax} stands for terminal relaxation time. Solid triangles and solid lines of matching colors are for linear samples PS-84k (blue color, left-pointing triangles) and PS-185k (green color, right-pointing triangles); empty triangles and dotted lines of matching colors are for rings PS-84k (blue color, left-pointing triangles) and PS-185k (green color, right-pointing triangles). Dashed red lines represent the best fits for every sample according to formula 1, with the shear thinning exponent used as the only fitting parameter. The best fit results are indicated in the figure for each sample, and overall, $\alpha_{\text{linear}} = 0.89 \pm 0.05$ and $\alpha_{\text{ring}} = 0.56 \pm 0.02$. The numerical values of τ_{relax} and η_0, used to normalize both axes, were determined in oscillatory experiments (see Figure 3), and as a proxy for η_0, we simply used the value obtained at the smallest accessible frequency; more details and data on this are found in Table S1 in the Supporting Information.

polymer are connected additionally by the finitely extensible nonlinear elastic (FENE) potential defined as $U_{\text{bond}}(r) = -0.5kR_0^2\ln(1 - (r/R_0)^2)$ for $r < R_0$ and $U_{\text{bond}}(r) = +\infty$ for $r > R_0$, with $k = 30\varepsilon/\sigma^2$ and $R_0 = 1.5\sigma$. A bond bending potential $U_B(\theta) = k_\theta(1 + \cos\theta)$ is applied, where θ is the angle between two consecutive bonds in a polymer and $k_\theta = 1.5\varepsilon$. For more details on potentials and parameters, see ref 5. The number of beads in an entanglement strand of such a linear polymer chain is $N_e = 28 \pm 1$.[46,47]

The samples of nonconcatenated ring polymers and the samples of linear polymers are identical to those in the previous simulations.[5,10] A melt sample contained 200 rings or between 250 and 2500 linear chains in a simulation box. Periodic boundary conditions were applied in all three directions. The melts were prepared and equilibrated at density $\rho = 0.85\sigma^{-3}$ and temperature $T = 1.0\varepsilon/k_B$. The number of monomers in a polymer was $N = 100, 200, 400$, and 800 for the samples of linear chains and $N = 100, 200, 400, 800$, and 1600 for the rings. Using $N_e = 28$, these polymerization degrees correspond to $Z = N/N_e = 3.6, 7.1, 14.3, 28.6$, and 57.1, respectively.

In the present work, nonequilibrium molecular dynamics simulations (NEMD) are performed to determine the steady-state shear viscosity η as a function of the shear rate $\dot{\gamma}$. We integrated the equations of motion traditionally called SLLOD,[56−58] the standard set of first-order linear differential equations for NEMD simulations of homogeneous planar shear flow, with a Nosé−Hoover thermostat. We are aware that imposing homogeneous planar shear flow could suppress inhomogeneous flow instabilities, if they exist. This suppres-

sion is justified by the agreement of our computational results with experiments. Previous NEMD simulations for linear chains[59−61] were for fully flexible chains ($k_\theta = 0$, with a Kuhn segment of 1.8σ, see ref 62). Here, we present new results for linear and ring polymer melts for stiffer chains, with $k_\theta = 1.5\varepsilon$ and Kuhn segment $b = 2.8\sigma$. The flow velocity v_x along the x direction depends linearly on the y coordinate with a constant shear rate $\dot{\gamma} = \partial v_x/\partial y$, as shown in Figure 2. The Nosé−Hoover thermostat maintains the temperature at $T = 1.0\varepsilon/k_B$ with a temperature damping factor of $10\tau_{\text{LJ}}$. The flow reaches a steady state at shear strain γ of order $10 \div 20$. The steady-state viscosity η is computed as the ratio of shear stress and the shear rate $\dot{\gamma}$.

Simulation Results. The unique topology of non-concatenated ring polymers gives rise to distinctive conformational and dynamic properties.[4,5,7−10,30,63−67] Previous simulations[5,10] have compared the properties of ring polymers and linear polymers in entangled melts. For the rings, the mean squared radius of gyration $\langle R_g^2 \rangle$ was found to scale with the number of monomers in a polymer as $N^{2/3}$ in the limit of large N, indicating a compact conformation.[5] This is in contrast to the Gaussian random-walk conformations of linear polymers with $\langle R_g^2 \rangle \sim N$. The ring polymers were found to diffuse faster than the linear polymers of the same N (see ref 10 and also some pertinent experimental data in ref 68). The stress relaxation modulus $G(t)$ of rings does not exhibit a rubbery plateau, which is characteristic of entangled linear polymers. The zero shear viscosity of a ring polymer melt was found to vary as $\eta_0 \sim N^{1.4 \pm 0.2}$, which is a much weaker N dependence than $\eta_0 \sim N^{3.4}$ of entangled linear polymers[10] (compare also refs 63 and 69).

Figure 5 shows the shear rate dependence of viscosity $\eta(\dot{\gamma})$ for different polymers; this figure is the direct simulation analog of experimental Figure 3. The most obvious features of the data is that, first, viscosity of rings shear thins less drastically than viscosity of linear polymers and, second, longer polymers, in both rings and linear chains, have lower viscosity
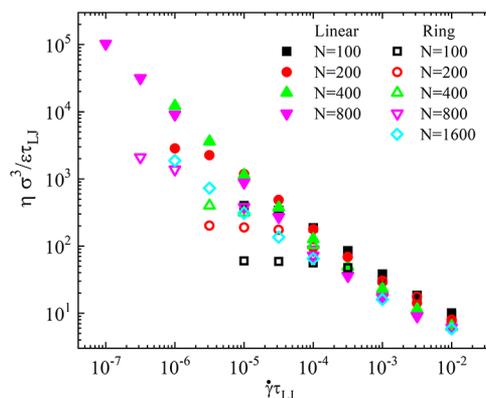
Figure 5. Nonequilibrium molecular dynamics (NEMD) simulation data on the steady-state shear viscosity η as a function of the shear rate $\dot{\gamma}$ for linear and ring polymers with indicated values of the polymerization degree, N. This figure is the direct simulation counterpart of experimental Figure 3. As in experiments, simulations show how viscosities of different samples approach one another at moderate shear rates, but then, longer chains shear thin more drastically than shorter chains, as explained below based on the shear slit model. The numerical data presented in this figure are listed for linear polymers and ring polymers in Tables S4 and S5 in the Supporting Information.
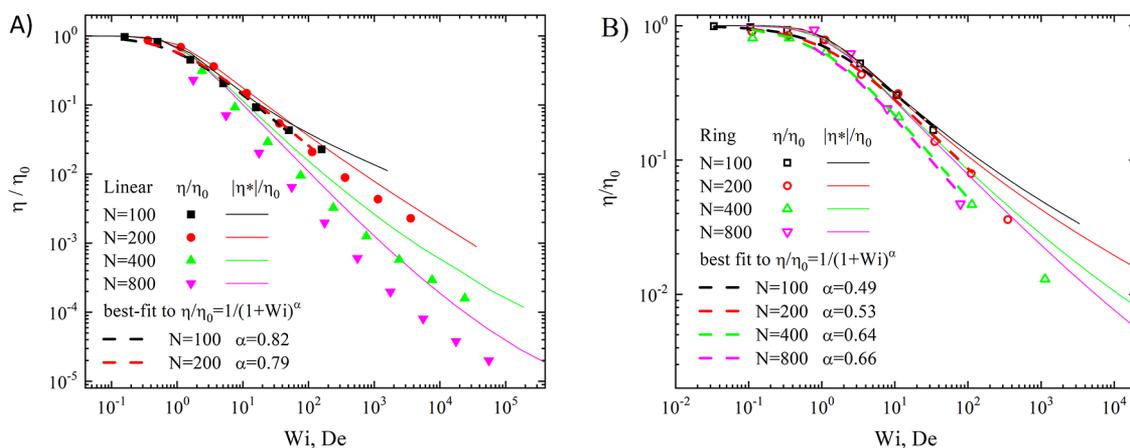
Figure 6. Steady shear viscosity, normalized by zero shear viscosity η_0, as a function of the Weissenberg number $Wi = \dot{\gamma}\tau_{\text{relax}}$, for different chain lengths N, shown by various filled symbols in figure A for linear chains and in open symbols in figure B for rings. Quantities η_0 and τ_{relax} used to normalize both axes were determined in independent equilibrium simulations; they are listed in Table S1 in the Supporting Information. We do not include in this figure the $N = 1600$ rings' data because we were unable to obtain a reliable estimate of η_0 from equilibrium simulations. Thin lines of matching colors show normalized absolute values of complex viscosity $|\eta^*(\omega)|$ computed from analytical interpolation expressions for the time-dependent relaxation modulus (see the Supporting Information, eq S2 for linear chains and eq S1 for rings, the latter taken from ref 9); deviations of these lines from the data at large shear rates indicate failure of the Cox–Merz rule. Thick dashed lines of matching colors represent the best fit according to eq 1, with the shear thinning exponent α as a fitting parameter. The best fit values of α are indicated in the figure, and overall, $\alpha_{\text{linear}} = 0.80 \pm 0.06$ and $\alpha_{\text{rings}} = 0.57 \pm 0.08$ (although data suggest that there could be an upward trend of α with increasing N for rings but not for linear chains). This figure is the direct simulation counterpart of experimental Figure 4.

than shorter ones. Qualitatively, these trends are the same as in experiments.

To examine the universal shear thinning behavior, as in the experimental case, we rescale both vertical and horizontal axes and present in Figure 6 the normalized viscosity $\eta(\dot{\gamma})/\eta_0$ as a function of the Weissenberg number $Wi = \dot{\gamma}\tau_{\text{relax}}$. We emphasize that both η_0 and τ_{relax} are not fitting parameters; they are measured (computed) in an independent simulation run (reported in ref 10), in complete analogy with the procedure in experiments. While $\eta(\dot{\gamma})$ is computed by imposing a shear rate and observing the resulting stress, η_0 and τ_{relax} are found without any imposed shear, by running equilibrium simulation, observing fluctuating stress, and using Green–Kubo relations (the results of this procedure are listed in Table S1 in the Supporting Information). We separately fit the resulting curves for each N, to formula 1, which describes the crossover from $\eta = \eta_0$ in the zero rate limit to the shear thinning regime with $\eta \sim \dot{\gamma}^{-\alpha}$ as Wi increases above unity. As in experiments, α is the only fitting parameter. The best fit results are shown in Figure 6. At modest Wi, all curves for different N are reasonably close (given the errors incurred by independently measured η_0 and τ_{relax}); this is certainly true for $N \geq 400$ and for all N at $Wi \leq 10$. The overall averaged "universal" shear thinning exponent can be estimated to be $\alpha = 0.80 \pm 0.06$ for linear chains and $\alpha = 0.57 \pm 0.08$ for rings, in agreement with experiments. At larger shear rates, behavior is no longer universal, even approximately, with more rapid shear thinning for longer chains than for shorter ones.

■ THEORETICAL TREATMENT

Naive Scaling Theory of Shear Thinning. To understand the rich phenomenology observed in both experiments and simulations, we develop below simple scaling theory of shear thinning. In this theoretical part, we focus mostly on rings, for two reasons. First, it is less studied. Second, somewhat surprisingly, it is simpler because for linear chains, the dynamics is (approximately) self-similar only up to the

number of monomers in one entanglement strand N_e, above which the tube suppresses relaxation modes, while rings for $N > N_e$ cross over to another regime, which is also self-similar (although there is no complete understanding at present as to whether self-similarity extends all the way to $N \to \infty$, or there is a glassy state above some value of N/N_e, see refs 66 and 70).

First, consider the regime of a very low shear rate $\dot{\gamma} \to 0$, and let η_0 be the corresponding zero shear rate viscosity (i.e., consider the linear response regime). We estimate zero shear rate viscosity as

$$\eta_0 = \int_0^\infty G(t)\,\mathrm{d}t \simeq \int_0^{\tau_{\text{relax}}} G(t)\,\mathrm{d}t \sim \frac{k_B T}{N\nu}\tau_{\text{relax}} \quad (2)$$

The first part of this relation is the exact expression of zero shear rate viscosity in terms of the stress relaxation modulus $G(t)$; it shows that all dynamical modes of the system contribute to dissipation. This integral is controlled by the terminal relaxation time τ_{relax}, integration can be cut off at τ_{relax}, and therefore, the integral is estimated as the product of the terminal modulus and τ_{relax}. The terminal modulus for entangled unconcatenated rings is about $k_B T$ per volume $N\nu$ occupied by one molecule (with ν volume per monomer); note that this is very different from entangled linear chains, where it would be $k_B T$ per entanglement, and the difference is exactly due to the lack of a rubbery plateau for rings. For the τ_{relax}, we use $\tau_{\text{relax}} \simeq \tau_e(N/N_e)^{7/3}$ for $N > N_e$, which is the result of the work of Ge et al.[9] yielding

$$\eta_0 \simeq \frac{k_B T}{N_e \nu}\tau_e\left(\frac{N}{N_e}\right)^{4/3} \quad (3)$$

Here $\tau_e = \tau_0 N_e^2$ is relaxation time of the chain section of N_e monomers, and τ_0 is a monomer relaxation time.

Up to this point, we discussed zero shear rate viscosity η_0. For shear rates $\dot{\gamma} < 1/\tau_{\text{relax}}$, viscosity $\eta(\dot{\gamma})$ should be close to η_0. For a polymer molecule in a stronger steady shear flow, with the shear rate $\dot{\gamma} > 1/\tau_{\text{relax}}$ beyond the linear response regime,

the time scale $\tau_s = \dot{\gamma}^{-1} < \tau_{relax}$ corresponds to a relaxation time of a subsection of a ring containing some $g_s < N$ monomers. The size of this subsection sets the length scale, ξ_s, that is smaller than the entire polymer. This length scale defines the size of shear blobs—maximal polymer sections that can relax during time $\dot{\gamma}^{-1}$. Polymer sections with relaxation time shorter than τ_s remain in equilibrium (even though we show later that it is only a constrained equilibrium consistent with stretching in the velocity direction) and should be described by the results for sizes and relaxation times of chain sections in an equilibrated ring melt[9]

$$\frac{\xi(g)}{b} \simeq \begin{cases} g^{1/2} & \text{for } g < N_e \\ N_e^{1/2}(g/N_e)^{1/3} & \text{for } g > N_e \end{cases};$$

$$\frac{\tau(g)}{\tau_0} \simeq \begin{cases} g^2 & \text{for } g < N_e \\ N_e^2(g/N_e)^{7/3} & \text{for } g > N_e \end{cases} \quad (4)$$

From $\tau(g_s) = \tau_s = \dot{\gamma}^{-1}$, we find

$$g_s \sim \begin{cases} N_e(\dot{\gamma}\tau_e)^{-3/7} & \text{for } \dot{\gamma}\tau_e < 1 \\ N_e(\dot{\gamma}\tau_e)^{-1/2} & \text{for } \dot{\gamma}\tau_e > 1 \end{cases},$$

$$\frac{\xi_s}{b} \sim \begin{cases} N_e^{1/2}(\dot{\gamma}\tau_e)^{-1/7} & \text{for } \dot{\gamma}\tau_e < 1 \\ N_e^{1/2}(\dot{\gamma}\tau_e)^{-1/4} & \text{for } \dot{\gamma}\tau_e > 1 \end{cases} \quad (5)$$

To estimate the shear viscosity of the melt, we make an additional conjecture: while zero shear viscosity is contributed by all modes and is dominated by terminal relaxation time of the chain (see eq 2), we argue that in the nonlinear regime, dissipation is only due to thermally equilibrated modes of the chain on length scales up to shear blobs or on time scales up to $1/\dot{\gamma}$. This conjecture is mathematically expressed as

$$\eta(\dot{\gamma}) \simeq \int_0^{1/\dot{\gamma}} G(t)dt \equiv \tilde{\eta} \quad (6)$$

This restricted integral up to $1/\dot{\gamma}$ is actually an alternative way of presenting a Cox–Merz-like conjecture. In our view, this formulation is physically better justified than the traditional one based on the absolute value of complex viscosity since the absolute value does not have any clear physical significance and contains contribution not only from viscous but also from elastic components of stress relaxation. Mathematically, though, for a broad class of $G(t)$ functions, the restricted integral (eq 6) with an upper limit replaced by $1/\omega$ and denoted by us as $\tilde{\eta}(\omega)$ is within ~15% of the "classical" absolute value of complex viscosity $|\eta^*(\omega)|$ (see Figure S8 in the Supporting Information).

Below, we will return to the detailed analysis of this assumption, but for now, let us accept it and explore its consequences. To estimate viscosity for rings based on the restricted integral (eq 6), we say that the shear modulus is on the order of thermal energy k_BT per volume $g_s v$ occupied by g_s monomers of a shear blob, while relaxation time of this blob is, by definition, the upper limit of the integral (eq 6), $\tau_s = 1/\dot{\gamma}$. As a result, the shear blob conjecture leads to the following prediction for shear viscosity

$$\eta(\dot{\gamma}) \sim \frac{k_BT}{g_s v}\tau_s \sim \begin{cases} \dfrac{k_BT\tau_0}{v}N_e(\dot{\gamma}\tau_e)^{-4/7} & \text{for } \dot{\gamma}\tau_e < 1 \\ \dfrac{k_BT\tau_0}{v}N_e(\dot{\gamma}\tau_e)^{-1/2} & \text{for } \dot{\gamma}\tau_e > 1 \end{cases} \quad (7)$$

Note that this viscosity is N-independent. The most interesting is the regime with a shear blob larger than the entanglement length but smaller than the entire chain, $N_e < g_s < N$; the corresponding result can be rewritten in the form

$$\eta(\dot{\gamma}) \sim \eta_0(\dot{\gamma}\tau_{relax})^{-4/7}, \quad \text{valid for } 1/\tau_{relax} < \dot{\gamma} < 1/\tau_e \quad (8)$$

The same result (eq 8) can be also understood using either the traditional or our modified formulation of the Cox–Merz rule. The starting point of this analysis is the stress relaxation modulus $G(t)$ for the melt of unconcatenated entangled rings, which was derived in ref 9 to scale (in the relevant time interval between τ_e and τ_{relax} as $G(t) \simeq G_e(t/\tau_e)^{-\beta}$, with $\beta = 3/7$. From here, we can determine that the complex viscosity at frequency ω, $\eta^*(\omega) = \int_0^\infty G(t)e^{i\omega t}dt$, is proportional to $\omega^{\beta-1}$, and replacing $\omega \rightarrow \dot{\gamma}$ as per Cox–Merz prescription, we exactly reproduce the result (eq 8) for the shear thinning exponent $\alpha = 1 - \beta = 1 - 3/7 = 4/7$. The same result is of course also obtained from our restricted integral $\tilde{\eta}$ (eq 6).

Scaling results from eqs 7 and 8 are plotted in Figure 7.
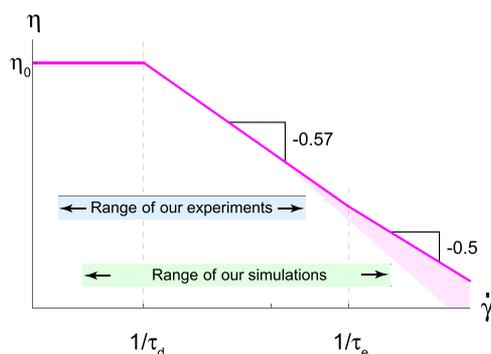
Figure 7. Scaling theory prediction for shear viscosity as a function of the shear rate, in a double logarithmic scale. This plot is to be compared with Figure 8 summarizing experimental and simulation data. The plot is presented for one particular N. With changing N, the value of η_0 (viscosity in the linear regime at very small $\dot{\gamma}$) increases. At larger $\dot{\gamma}$, the curve is universal, and viscosity does not depend on N. Also, at even larger $\dot{\gamma}$, viscosity deviates downward from the universal curve as indicated by the colored wedge. This wedge starts at the shear rate where tension blobs become as small as comparable to one Kuhn segment, in which case Kuhn segments start to partially orient along the flow, further reducing the viscosity; see Figure 10 for further details about this. Note the encouraging consistency of this effect with observations in Figures 4 and 6.

Experimental and Computational Tests of Naive Theory. The main result of our scaling theory based on the shear blob conjecture—eq 8, with the shear thinning exponent $\alpha = 4/7 \approx 0.57$—is in at least a satisfactory agreement with both experimental and simulation results for the melt of rings, as presented above in this paper. Note that both our experimental and simulation results definitely extend to shear rates $\dot{\gamma} > 1/\tau_{relax}$ (see Figures 4 and 6, respectively), but experimental data remain at $\dot{\gamma} < 1/\tau_e$ (the latter estimated at $1/\tau_e \approx [500 \div 1000]$ s^{-1}, see Figure 3), while simulation data approach or even go slightly beyond that point (given that $1/\tau_e \sim 10^{-3}/\tau_{LJ}$, see

Figure 5). Formula 7 also predicts that at a higher shear rate $\dot{\gamma} > 1/\tau_e$, the shear thinning exponent crosses over from 4/7 to 1/2; this prediction remains to be tested.

Beyond the agreement on a single number, a more sensitive test, directly addressing our key assumption eq 6 against experimental and computational data, is presented in Figure 8.
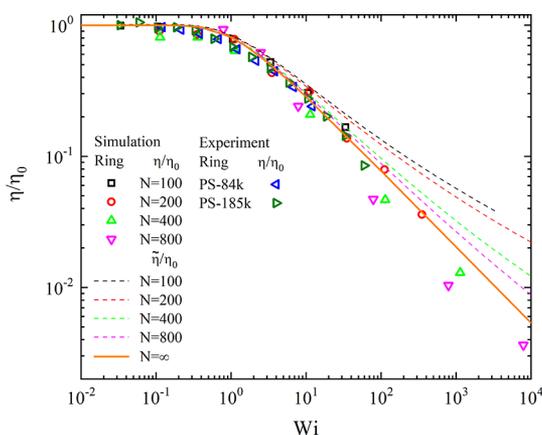
Figure 8. Jointly plotted data of experiments and simulations for the steady shear viscosity, normalized by the zero shear rate viscosity, as a function of the Weissenberg number, for entangled rings. Experiments and simulations agree very well. Note that scale factors η_0 and τ_{relax} were determined via separate experimental or computational measurements for every sample and every N, and no joint fitting is involved to align the results. Thin dashed lines of matching colors for every N represent quantity $\tilde{\eta}$ defined by the incomplete integration (eq 6), where $G(t)$ was taken from previous zero shear simulations (ref 10) interpolated by an analytical formula derived in ref 9 (formula A.2 in their Supporting Information, reproduced in eq S1; a thick solid orange line, with the slope of $-7/12$, represents the limit of $\tilde{\eta}/\eta_0$ for $N\rightarrow\infty$, derived in the Supporting Information, formula S5.

First of all, we see more than a satisfactory agreement between experiments and simulations (further confirming the insignificance of linear chain contamination of our experimental ring samples). Importantly, this agreement is achieved without any fitting at all because scale factors η_0 and τ_{relax} were not adjusted but rather measured in independent experiments (on linear viscoelasticity, see Figure 2 above) or independent simulations (from fluctuations in an equilibrated system, see ref 10). Dashed thin lines in the same figure represent plots, for every N in matching colors with data symbols, the quantity $\tilde{\eta}/\eta_0$ for computationally determined $G(t)$ (using the interpolation formula derived in ref 9 and reproduced in the Supporting Information, eq S1). Although data agree reasonably well with these curves at moderate shear rates, $Wi \lesssim 10$, confirming for this range both our naive scaling conjecture and the Cox–Merz rule, the disagreement grows dramatically at larger values of Wi. In fact, the decrease in slope for $\tilde{\eta}$ (or for $|\eta^*|$) with increasing Wi is natural for a number of reasons. Indeed, as increasing Wi (or De) approaches τ_{relax}/τ_e, short wavelengths of Rouse and undulation modes start contributing. As they correspond to steeper slopes of $G(t)$ (on a log–log plot) than entanglement modes for ring melts, this implies more shallow $\tilde{\eta}$ (or $|\eta^*|$) slope (again, on a log–log plot). However, surprisingly, real data deviate from the $\tilde{\eta}$ curves in the opposite direction. Moreover, shear thinning in the large Wi regime is stronger than $\tilde{\eta}$ even for the $N\rightarrow\infty$ limit (thick solid orange line in the figure). This suggests the existence of some mechanism preventing certain dynamical modes of polymers

from taking part in dissipation. This represents major complication for naive scaling theory and requires a deeper look into the conformations and dynamics of rings in the strongly nonlinear regime.

Conformations and Dynamics of Rings in a Shear Flow. Although the shear blob conjecture for a ring polymer melt led us to a success explaining the value of the shear thinning exponent $\alpha = 4/7$, it also raises several questions. Most importantly, why does larger scale motion appear not to contribute to dissipation? Why does universal power law shear thinning break down at higher Wi? In short, even though this simple scaling argument successfully predicts the shear thinning exponent α, do we satisfactorily understand the phenomenon in terms of conformations and dynamics of the macromolecules?

Shear Slit Model. To find answers to these questions, we examined in greater details the numerical simulation results and arrived at the following description, schematically depicted in Figure 1. Every ring, for instance, magenta in Figure 1, in the strong ($\dot{\gamma} > 1/\tau_{relax}$) shear flow is dynamically confined in the velocity gradient direction y within the distance of the order of the shear blob size ξ_s. The neighboring chains above and below, like blue and green in Figure 1, slide past our chosen (magenta) chain with the speed of the order of $\sim\dot{\gamma}\xi_s$. Simultaneously, every chain, when averaged over time, is also strongly stretched by the flow in the x direction, elongated much more strongly than due to pure confinement in the y direction. This stretching results in formation of tension blobs, of $g_t < g_s$ monomers each. Thus, the central point of this emerging description is the presence of two distinct length scales, ξ_s and ξ_t, or two blob types, with g_s and g_t monomers in the velocity gradient and the flow directions, respectively. In this sense, our picture is reminiscent of a chain confined in a capillary and simultaneously stretched by a sufficiently strong force along the capillary, such that tension blobs are smaller than capillary diameter. In this pulling-inside-a-capillary model, each confinement blob is a Gaussian chain of several tension blobs extended in the direction of the applied tension force, transverse fluctuations of which are confined by the capillary. Our shear flow situation is different from the capillary model only in two aspects. First, while a typical capillary may have a round cross section, we deal with a highly asymmetric capillary or simply a slit that strongly confines a polymer in the y (velocity gradient) direction and not in the z (vorticity) direction. Second, the fractal structure of confinement blobs is not Gaussian but that of a fractal globule. Since shear blobs are aligned along the flow direction, relative velocity of different parts of the chain is smaller than $\sim\dot{\gamma}\xi_s$, which is why longer wavelength modes than shear blob size do not contribute to the dissipation. Indeed, dissipation in general is controlled by the relative velocity of different parts of the same chain, which is slower than $\dot{\gamma}[y_{max} - y_{min}]$, where y_{max} and y_{min} are maximal and minimal y coordinates among all monomers of a given chain. By suppressing long wavelength modes, the system limits chain spread along the y direction to just about ξ_s. In turn, this also explains why the Cox–Merz rule is, roughly, applicable to our shear slit model.

To clarify the above description, it is useful to consider the following scaling estimate of the relation between the sizes of the two types of blobs. Since relative velocity of different parts of the polymer is $\sim\dot{\gamma}\xi_s$, the force acting in the velocity direction on one shear blob is $\sim\dot{\gamma}\xi_s\zeta(g_s)$, where $\zeta(g)$ is the friction coefficient for a chain section of g monomers. With N/g_s blobs,
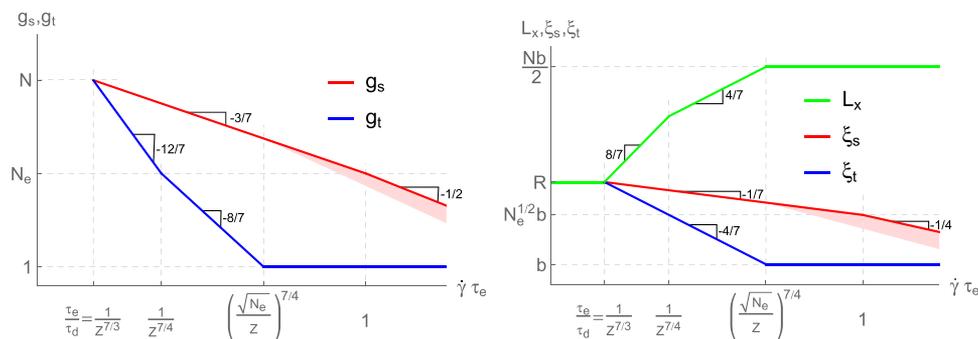
Figure 9. Shear rate dependencies (on a double logarithmic scale) of numbers of monomers in shear and tension blobs, g_s and g_t, their sizes ξ_s and ξ_t, and polymer size along the flow x direction, $L_x \simeq (N/g_t)\xi_t$. The plots are shown for $N > N_e^{3/2}$; a similar figure for the opposite case can be found in the Supporting Information, Figure S3. When the tension blob becomes as short as one Kuhn segment, a further increase in the shear rate leads to Kuhn segments increasingly orienting along the flow and reducing the shear blob size. Since we do not analyze this process in detail, we show this region as a colored wedge of increasing width.

the total drag force stretching the chain is about $f \sim \dot{\gamma}\xi_s\zeta(g_s)N/g_s$. For this force estimate, it is important to realize that the confining slit is slightly tilted with respect to the flow direction, resulting in drag force acting on one half of the chain mostly in the positive x direction and on the opposite half mostly in the negative x direction, as depicted in Figure 1. Of course, this implies a certain profile of tension force, gradually dropping toward the largest and smallest x, but this does not affect the scaling estimate. Tension force f generates tension blobs of the size $\xi_t = k_\mathrm{B}T/f$ (our simulations suggest that there is enough time for the chain to sample conformations by means of longitudinal modes to generate entropic force; see below). Thus, we arrive at the following relation between sizes of blobs ξ_s and ξ_t

$$\frac{b}{\xi_t} \sim \tau_0\dot{\gamma}\frac{\xi_s}{b}\frac{\zeta(g_s)}{\zeta_0}\frac{N}{g_s} \tag{9}$$

Here, we used $\tau_0 = \zeta_0 b^2/k_\mathrm{B}T$ with ζ_0 the Kuhn monomer friction coefficient. To give this relation a more explicit form, we use the results (eq 4) for the sizes and relaxation times of chain sections in a fractal globule[9] and also the related result for the friction coefficient of the subchain (which can be recovered from eq 4 by stating that the chain section of g monomers should, at equilibrium, diffuse at a distance $\sim\xi(g)$ during time $\tau(g)$)

$$\frac{\zeta(g)}{\zeta_0} \simeq \begin{cases} g & \text{for} \quad g < N_e \\ N_e(g/N_e)^{5/3} & \text{for} \quad g > N_e \end{cases} \tag{10}$$

Plugging this into eq 9, we can find how blob sizes ξ_s and ξ_t, as well as monomer numbers g_s and g_t, depend on the shear rate $\dot{\gamma}$. The specific scaling relations resulting from this analysis are provided in Table S6 for $N > N_e^{3/2}$ and Table S7 for $N < N_e^{3/2}$ in the Supporting Information.

Here, we will concentrate on the long chains with $N > N_e^{3/2}$ because it is relevant for simulations with $N \gtrsim 150$ and for experiments with PS at $M \gtrsim 100$ kg/mol. Note that in the most interesting case, when the tension blob is smaller than entanglement length but still larger than a monomer ($N_e > g_t > 1$) while shear blob is larger than entanglement length ($g_s > N_e$), there is the following relation between shear and tension blobs

$$g_t \simeq g_s^{8/3}N_e^{1/3}/N^2 \quad \text{for} \quad 1 < g_t < N_e \tag{11}$$

This result can be instructively rewritten as $g_t \simeq g_s(g_s/N)^{5/3}(N_e/N)^{1/3}$, showing that indeed, $g_t < g_s$. Dependencies of blob sizes and monomer numbers on the shear rate $\dot{\gamma}$ are summarized in Figure 9. What we see is that with an increasing shear rate, once $\dot{\gamma}\tau_\mathrm{relax} > 1$, tension blobs decrease. Specific scaling of this decrease changes when g_t becomes smaller than N_e, but a much more important quantitative change happens when the tension blob decreases to about the size of a Kuhn monomer, with g_t and ξ_t/b approaching unity. This happens at $\dot{\gamma}\tau_e \sim (N_e^{3/2}/N)^{7/4}$, which is still at $\dot{\gamma}\tau_e < 1$ (for $N > N_e^{3/2}$). The situation changes upon a further increase in the shear rate $\dot{\gamma}$, because further stretching the chain leads to individual Kuhn segments increasingly orienting along the flow, which in turn reduces the size of shear blobs in the gradient direction through nonlinear coupling between flow and velocity gradient directions. Note that orientation of Kuhn segments along the flow direction makes its projection in the velocity gradient direction smaller, thus reducing polymer size in the velocity gradient direction. In this regime, our theory needs to be properly corrected, which we indicate by the colored wedge of uncertainty in Figure 9.

Another way to look at the shear slit model predictions is by considering x, y, and z components of the end-to-end vectors for chain sections of k bonds (see cartoon in Figure 10), as a function of k. Corresponding predictions of the model are summarized in Figure 11.
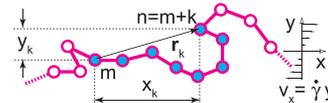
Figure 10. End-to-end vector $\mathbf{r}_k$ of a chain section of k bonds, between monomers m and $n = m + k$, and its components, easily measured in computation and an informative characteristic of the system.

Below, we compare the predictions of the shear slit model to simulation data.

Experimental and Computational Evidence Supporting the Shear Slit Model. One important success of our shear slit model is its natural explanation of the observed normal stress differences in the shear flow of unconcatenated entangled rings. As a reminder (see, e.g., a book[71]), two normal stress differences are defined in terms of the components of the deviatoric (trace-free) part of the stress tensor σ_{ij} as follows: N_1
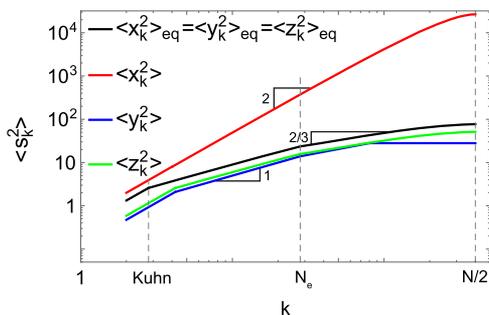
Figure 11. Theoretical prediction for the mean square chain section sizes in the x, y, and z directions as a function of section length (the number of bonds) k. In making this plot, we assumed the computer simulation values of the Kuhn segment $b = 2.8$ and $N_e = 28$. For ring polymers in question, there is an obvious symmetry $\langle s_k^2 \rangle = \langle s_{N-k}^2 \rangle$; therefore, we show only the plot up to $k = N/2$, where all curves have maxima (s is either x, y, or z). The black line corresponds to the equilibrium situation, when all projections are the same; in this case, to enforce $k \leftrightarrow N - k$ symmetry, we use the interpolation formula $\langle s_k^2 \rangle_{eq} = 1/\left(\frac{1}{f(k)} + \frac{1}{f(N-k)} \right)$, where the auxiliary function $f(k)$ is defined to represent all physically expected scaling regimes, $f(k) \sim k^2$ up to one Kuhn segment length, followed by Gaussian $f(k) \sim k$ up to one entanglement length N_e and followed by the fractal globule compact scaling $f(k) \sim k^{2/3}$. Curves of other colors represent the predictions of the shear slit model for a shear rate close to the crossover value $\dot{\gamma} \tau_e \sim (N_e^{3/2}/N)^{7/4}$ (see Figure 9), where the tension blob is only a few Kuhn segments long, and Kuhn segments are partially oriented along the flow. For the x direction, we plot $\langle x_k^2 \rangle$ that results from the prediction of the completely stretched ring of N/g_t tension blobs (see corresponding auxiliary calculation in the Supporting Information, formula S9 and comments to it). For the y direction, $\langle y_k^2 \rangle$ behavior is similar to $\langle y_k^2 \rangle_{eq}$, with two modifications: first, effective straight segment size is enlarged because Kuhn segments are partially oriented; second, $\langle y_k^2 \rangle$ saturates when it hits the shear blob scale ξ_s^2. Finally, due to $k \leftrightarrow N - k$ symmetry, $\langle z_k^2 \rangle = 1/\left(\frac{1}{h(k)} + \frac{1}{h(N-k)} \right)$, where the auxiliary function $h(k)$ is $\sim k$ modified due to oriented Kuhn segments similar to $\langle y_k^2 \rangle$ followed by Gaussian and fractal globule regimes.

$= \sigma_{xx} - \sigma_{yy}$ and $N_2 = \sigma_{yy} - \sigma_{zz}$. Since the shear slit model implies chain compression in the y direction (velocity gradient) to about the shear blob size, σ_{yy} should be smaller than σ_{zz}, with the negative difference, N_2, controlled by the number of monomers in a shear blob g_s. By a similar logic, since the molecules are strongly stretched in the x (flow) direction, σ_{xx} should be larger than σ_{zz}, and the difference between them, which is $N_1 + N_2$, should be controlled by g_t, the number of monomers in one tension blob. Thus, we arrive at the estimates

$$N_2 \simeq -\frac{k_B T}{v g_s} \qquad N_1 + N_2 \simeq \frac{k_B T}{v g_t} \approx N_1 \qquad (12)$$

where v, as before, is volume per Kuhn monomer. Note that since g_t is significantly smaller than g_s, we predict that N_1 is significantly larger than N_2 (in absolute value) and has an opposite sign. While we postpone the detailed analysis of these predictions for another paper, we found them consistent with our data so far. In particular, since the volume per Kuhn segment is typically around 1 nm³ and $k_B T = 5.8$ pN·nm at 150 °C, the value of N_1 at the onset of the nonuniversal regime of shear thinning (where $g_t \gtrsim 1$) is predicted to be on the order of a few MPa. From Figure 4, this onset occurs at about $Wi \sim 30$ for the PS-185k ring, where the respective experimental value of N_1 is about 1 MPa.

Furthermore, comparing eq 12 with formula 7 for viscosity, $\eta \simeq \frac{k_B T}{v g_s} \dot{\gamma}^{-1}$, we arrive at the relation

$$\eta \simeq -N_2 \dot{\gamma}^{-1} \qquad (13)$$

which is also in a semi-quantitative agreement with our data (not shown), although we postpone the detailed analysis.

Another important prediction of the model is breaking of universality at large shear rates, as indicated by shaded wedge regions in theoretical plots in Figures 7 and 9. It is predicted to happen when the tension blob becomes as short as about one Kuhn segment, and partial orientation of segments starts reducing transverse sizes of shear blobs, progressively removing shorter and shorter scales from dissipation. The onset of this
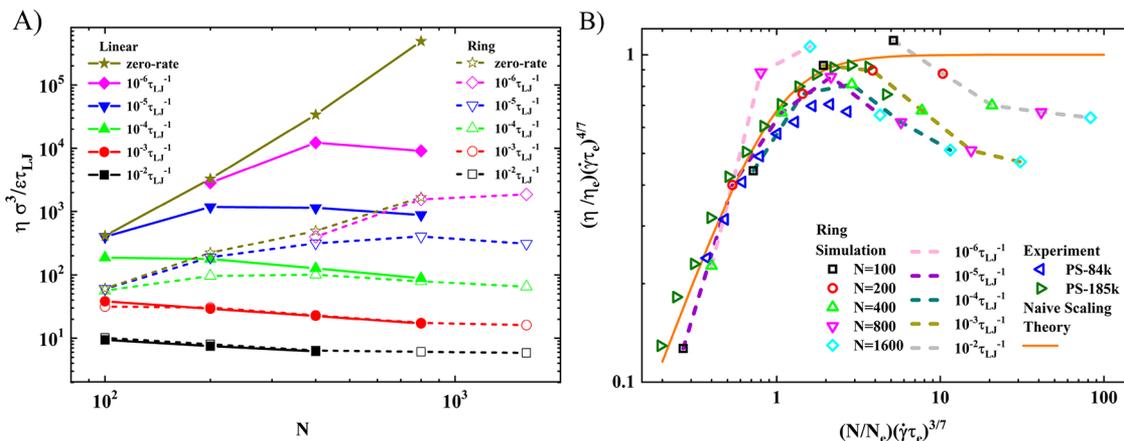
Figure 12. (A) Nonmonotonous behavior of steady shear viscosity as a function of chain length for both rings and linear polymers predicted by theory and observed in simulations. Note that at large shear rates, rings and linear polymers start behaving in a similar way, consistent with the idea that at $\dot{\gamma} \gtrsim 1/\tau_e$ topological constraints should be marginalized. (B) Same simulation data for rings replotted in reduced variables, imperfectly but reasonably collapsing all curves to a universal master curve as predicted theoretically (eq 14) and demonstrating the nonuniversal deviation downward from the master curve with growing either N or $\dot{\gamma}$. Experimental points included in this graph follow the same trend. The following numerical values of parameters were used for this plot: for simulations, $N_e = 28$, $\tau_e = 238 \tau_{LJ}$ (consistent with fitting formula S1c in the Supporting Information), and $\eta_e = 15 \varepsilon \tau_{LJ}/\sigma^3$; for experiments, $M_e = 16.8$ kg/mol, $\tau_e = 0.0015$ s, and $\eta_e = 0.8$ kPa s.

can be seen in experimental Figure 2, where as we pointed out, the dependencies of viscosity on the shear rate for different N approach one another at an angle suggesting that they will cross at still larger values of $\dot\gamma$, consistent with our theory prediction. Indeed, in simulations, which we were able to perform at significantly larger Wi, we do see this new regime fully developed, as in Figures 5, 6, and 8. Quantitatively, the onset of nonuniversal behavior is predicted to scale as $Wi = \dot\gamma\tau_d \sim N^{7/12}N_e^{7/24}$; more detailed and more accurate data will be required to test this prediction.

An unexpected consequence of these theoretical predictions, confirmed by simulations in Figure 12, is the nonmonotonous dependence of viscosity on chain length N, at any fixed nonzero shear rate. While we are all used to the idea that viscosity grows with N as a power law ($N^{3.4}$ for linear chains, $N^{1.4}$ for rings), which is true for linear viscoelasticity, in the nonlinear regime, the situation is very different. Naive scaling theory predicts viscosity that is independent of N in the nonlinear regime (as it can be interpreted as linear viscosity of a melt of shear blobs, see the first part of eq 7, consistent with both experiments (Figure 3) and simulations (Figure 5). When N increases at a fixed shear rate $\dot\gamma$, the system crosses over from the linear to nonlinear regime, and we can capture this crossover for rings if we use our naive theory (taking expressions for $\eta_0 = \eta_e(N/N_e)^{4/3}$ and $\tau_{\rm relax} = \tau_e(N/N_e)^{7/3}$ at $N > N_e$) to rewrite formula 1) as

$$\eta(\dot\gamma) = \frac{\eta_e\left(\frac{N}{N_e}\right)^{4/3}}{\left[1 + \dot\gamma\tau_e\left(\frac{N}{N_e}\right)^{7/3}\right]^{4/7}} \Rightarrow$$

$$\frac{\eta(\dot\gamma)}{\eta_e} \times (\dot\gamma\tau_e)^{4/7} = \frac{\left[(\dot\gamma\tau_e)^{3/7}\frac{N}{N_e}\right]^{4/3}}{\left[1 + \left[(\dot\gamma\tau_e)^{3/7}\frac{N}{N_e}\right]^{7/3}\right]^{4/7}}$$

(14)

That means plotting $\eta(\dot\gamma\cdot\tau_e)^{4/7}/\eta_e$ against $(\dot\gamma\cdot\tau_e)^{3/7}N/N_e$ is predicted to collapse the data for one master curve, which is seen to happen indeed in Figure 12B within the applicability range of naive theory. This universal dependence, which epitomizes naive scaling theory, grows and saturates with increasing either N or $\dot\gamma$, as it does happen in Figure 12B (see the orange line). At a further increase in either N or $\dot\gamma$, the nonuniversal regime kicks in because with increasing N, the chain gets stretched by an increasing force, with consequentially decreasing tension blobs eventually forcing chain orientation within tension blobs, thus affecting shear blobs according to the shear slit model, and viscosity data in Figure 12B starts going down. Furthermore, we predict the viscosity decrease to be nonuniversal, with higher shear rate "break off" later from this "universal curve", as observed. Note that this nonuniversal regime corresponds to the pink wedges in Figures 7 and 9. Along with simulation data, we included in Figure 12B also our experimental data, which successfully collapse on the same master curve.

We now go back to our computational data, but instead of just presenting the final result, which is viscosity as a function of the shear rate $\dot\gamma$, we extract more detailed information about chain conformations and dynamics.

We will mostly concentrate on the example of rings with $N = 800$ and the shear rate $\dot\gamma = 10^{-4}\tau_{\rm LJ}^{-1}$, because at smaller $\dot\gamma$,

nonlinear effects are not very well pronounced, while at larger $\dot\gamma$, the chain is closer to full elongation. We start by estimating the Weissenberg number for the chosen shear rate $\dot\gamma = 10^{-4}\tau_{\rm LJ}^{-1}$. Since $N_e = 28$ for our computational model, the scaling estimate of Rouse relaxation time on this scale would be $\tau_{\rm LJ}N_e^2 \approx 800\tau_{\rm LJ}$; in fact, extensive fitting to the data in ref 9 (see also formula S1 in the Supporting Information) yields about four times shorter time, $\tau_e = 240\tau_{\rm LJ}$ (because they are rings; we already used this in Figure 12B), which we will adopt for further estimates. Given this τ_e, relaxation time of the $N = 800$ ring in a melt is estimated as $\tau_{\rm relax} = \tau_e(N/N_e)^{7/3} \approx 6 \times 10^5\tau_{\rm LJ}$, in agreement with computational results reported by Halverson et al.[10] Therefore, the Weissenberg number for $\dot\gamma = 10^{-4}\tau_{\rm LJ}^{-1}$ is equal to $Wi = \dot\gamma\tau_{\rm relax} \approx 60$, meaning that the chosen shear rate is in the nonlinear regime.

The chosen shear rate $\dot\gamma = 10^{-4}\tau_{\rm LJ}^{-1}$ corresponds to $\dot\gamma\tau_e \approx 0.024$. This is significantly larger than $(N_e/N)^{7/4} \approx 0.003$ while smaller than, but pretty close to, $(N_e^{3/2}/N)^{7/4} \approx 0.05$. This means, according to Figure 9, that the shear blob should be expected to be an entangled object with $g_s > N_e$, while the tension blob should be pretty small, a few monomers only.

Knowing the value of $\dot\gamma\tau_e \approx 0.024$ for the chosen example, we can directly estimate the number of monomers g_s in a shear blob from the condition that the relaxation time of a shear blob must be equal $1/\dot\gamma$, yielding $g_s = N_e(\dot\gamma\tau_e)^{-3/7} \approx 138$; as expected, $g_s > N_e$ (as a reminder, $N_e = 28$ for our computational model). Shear blob size is then $\xi_s/\sigma = (N_eb/\sigma)^{1/2}(g_s/N_e)^{1/3} \approx 15$, where the Kuhn segment is taken to be $b = 2.8\sigma$.

Given the determined number of monomers in a shear blob, $g_s \approx 138$, we can estimate also the number of monomers in a tension blob from eq 11. In doing so, it makes sense to plug in $N/2 = 400$ instead of just N because a fully stretched ring can be at most $N/2$ bonds long. This yields then $g_t \approx 9$, in the expected range.

Let us now look at the measured properties of conformation geometry. Figure 13 shows (for rings with $N = 800$) the dependence on the shear rate $\dot\gamma$ of the three eigenvalues λ_1, λ_2, and λ_3 of the gyration tensor, proportional to mean squared averaged axes of an ellipsoid representing a molecular shape. To clarify, the sum $\lambda_1 + \lambda_2 + \lambda_3 = R_g^2$ is nothing else but the mean squared averaged gyration radius. As expected, with an
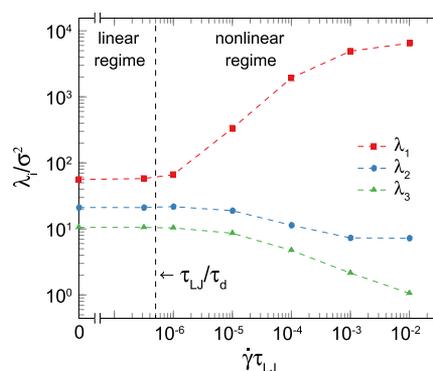
Figure 13. Computer simulation data for rings with $N = 800$ characterizing the geometry of conformations in terms of a (double logarithmic) plot of shear rate dependence for the three eigenvalues of the gyration tensor, proportional to mean squared axes of an ellipsoid representing polymer shapes λ_1, λ_2, and λ_3. Note that λ_1, λ_2, and λ_3 are different in the linear regime and even at $\dot\gamma = 0$; this is because they are not associated with specific spatial directions x, y, and z but rather represent the largest, intermediate, and smallest component of size.

increasing shear rate in the nonlinear regime $\dot{\gamma} > 1/\tau_{relax}$, molecules get strongly elongated in one direction (which becomes increasingly close to the flow direction x). Molecules also shrink in two transverse directions, with a representative ellipsoid (or triplet of eigenvectors) turning in a certain way in space. Specifically, when $\dot{\gamma} = 10^{-4}\tau_{LJ}^{-1}$, $\lambda_1 \approx 1900\sigma^2$ is very significantly larger than $\lambda_2 \approx 10\sigma^2$ and $\lambda_3 \approx 5\sigma^2$ (see further details of numerical data in Table S5 in the Supporting Information). Such a strong disparity between eigenvalues indicates that the molecules are strongly stretched along x, and we can estimate their length as $L_x = \sqrt{12\lambda_1} \approx 150\sigma$.

A more detailed view of the conformations is provided by another measure, presented in Figure 14. It shows computa-
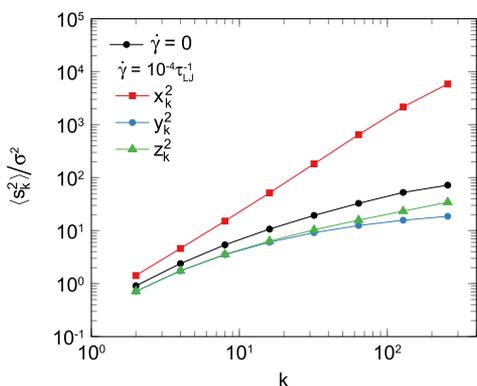
Figure 14. Computer simulation data for rings with $N = 800$ characterizing the geometry of conformations in terms of mean squared distance between monomers m and $n = m + k$ (see cartoon in Figure 10). These distances, averaged over m and over time, are plotted as a function of chain section length k, in a double logarithmic scale, for three directions, velocity direction $s = x$ (red squares), velocity gradient direction $s = y$ (blue circles), and vorticity direction $s = z$ (green triangles). The same mean squared distances in the equilibrium melt of rings without any shear are presented by black circles (the same in all three directions). This is to be compared with theoretically expected Figure 11.

tional data on the mean squared components $\langle x_k^2 \rangle$, $\langle y_k^2 \rangle$, and $\langle z_k^2 \rangle$ of the end-to-end vector of a chain section of k bonds (see cartoon in Figure 10), still at the shear rate $\dot{\gamma} = 10^{-4}\tau_{LJ}^{-1}$ (corresponding to $Wi = 60$); these quantities are plotted theoretically in Figure 11. As before, we see that shear leads to the x component (red squares) stretching and y and z components (blue and green symbols) shrinking compared to those at equilibrium (black circles). Furthermore, the value of $\langle x_k^2 \rangle$ for a half-ring, which is $\langle x_{N/2}^2 \rangle$, is very close to $8000\sigma^2$, and this is consistent with the above mentioned value of $\lambda_1 \approx 1900\sigma^2$ because $\langle x_{N/2}^2 \rangle = L_x^2/3 = 4\lambda_1$ for a ring stretched along one line (to clarify, there are inevitably two U-turn hairpins on a stretched loop, and two ends of the k-bond chain section can be on the opposite sides of the hairpin, making $\langle x_k^2 \rangle$ significantly smaller than $k^2\sigma^2$, smaller by a factor of 4 when $k = N/2$; see the Supporting Information, equation S10 for details).[5]

Since we know the length L_x, we can use this information to obtain another independent estimate of the tension blob size ξ_t and monomer number g_t. Assuming, for the sake of scaling estimate, that the stretch along x is uniform, distance $L_x \approx 150\sigma$ should be covered by $N/(2g_t)$ Gaussian ($\xi_t^2 = b^2 g_t$, with the Kuhn segment $b = 2.7\sigma$) tension blobs, of the x direction size $\xi_t/\sqrt{3} = \sqrt{2.7\sigma^2 g_t/3}$ each, i.e., $L_x = \frac{N\sigma}{2\sqrt{1.1g_t}}$, meaning that $g_t \approx 6$ and $\xi_t \approx 4\sigma$. As expected, tension blobs are small, each containing only a couple of Kuhn segments.

Based on the dynamics considerations, we estimated above $g_s \approx 138$, and then, shear slit model prediction (eq 11) gave us $g_t \approx 9$. Observing purely geometric properties of the molecules, we obtained now a new estimate $g_t \approx 6$. Both estimates are consistent to within a factor of 1.5. Of course, we should not have expected a quantitative agreement because the assumption of uniform stretching is a large oversimplification, and shear slit model prediction (eq 11) is derived via scaling, up to a numerical factor.

The above estimates are also consistent with the transverse dimensions of the chain, measured by $\langle y_k^2 \rangle$. Also, the observed
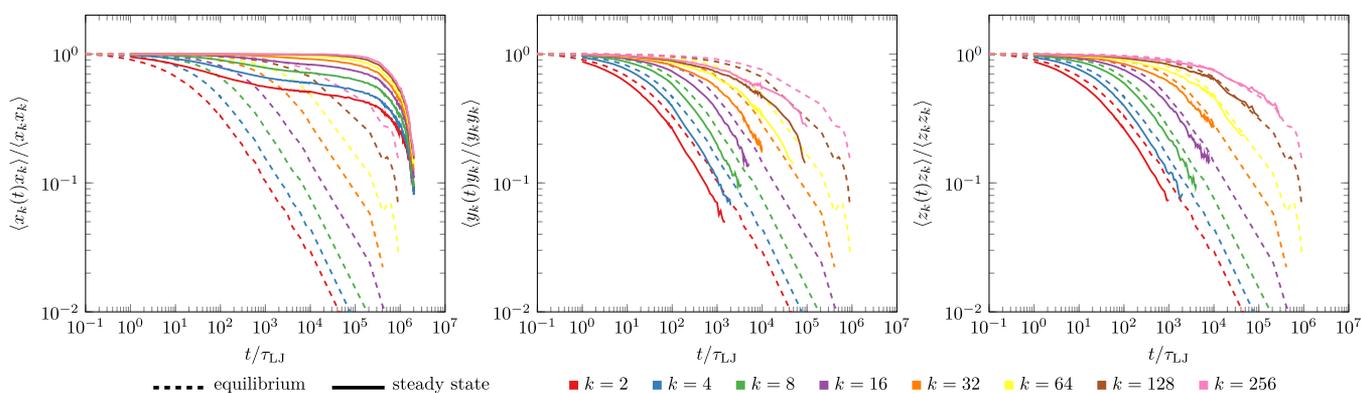
Figure 15. Time dependence of a normalized autocorrelation function between ends of a subsection consisting of k bonds for a ring of $N = 800$ in steady shear flow with $\dot{\gamma} = 10^{-4}\tau_{LJ}^{-1}$ in the x, y, and z directions, for various values of k from $k = 2$ to $k = 256$ (solid lines). Note that correlations of the x components of ring subsections persist much longer than at equilibrium (shown by dashed lines) followed by a sharp drop of correlation for x, almost independent of k, occurring at times much longer (about 100 times longer) than $1/\dot{\gamma}$. This drop of correlation is due to tumbling. For comparison, we also show in this figure time-dependent autocorrelation functions for the same chain sections of k monomers in equilibrium, at $\dot{\gamma} = 0$ (dashed lines). Note that correlations in x components exhibit dramatically more significant deviation from equilibrium than y and z components. As theory predicts, for subchains longer than shear blobs, $k > g_s$ (as a reminder, the latter is estimated above to be $g_s \approx 83$), autocorrelations of z components decay nearly identical to equilibrium (no effect of flow in the shear slit model to dynamics in the z direction), while in the y direction, even the longest subchains decorrelate faster than in equilibrium. This is consistent with the fact that in Figure 15, the largest difference between y and z directions is observed at $k > g_s$.

dependence of $\langle y_k^2 \rangle$ on k shown in Figure 14, given that the tension blob g_t is only a couple of Kuhn segments long, is consistent with theoretical expectations summarized in Figure 11.

We now turn to the dynamics of rings in a shear flow. We examine it by looking at time dependence of components of the same end-to-end vector $\mathbf{r}_k(t)$ for a chain section of k bonds, between monomers m and $n = m + k$ (see cartoon in Figure 10). Previously, we considered $\langle s_k^2 \rangle$, with s either x, or y, or z components of $\mathbf{r}_k$, averaging it over both m and time; now, we consider a time-dependent autocorrelation function defined as $\langle s_k(t)s_k(0) \rangle / \langle s_k^2 \rangle$, where average is now taken over m and over initial time. Figure 15 shows time dependence of these autocorrelation functions for all three components, x, y, and z, for one specific value of the shear rate, $\dot{\gamma} = 10^{-4}\tau_{LJ}^{-1}$. The autocorrelation function is normalized by its value at $t = 0$, which is why all curves in Figure 15 begin from unity. For comparison, we also show in the same figure autocorrelation in equilibrium (dashed lines). The data confirm the dramatic difference in dynamics between longitudinal (x) and transverse directions. The autocorrelation function for the x direction remains close to unity, almost independent of k, for the time about $10^6\tau_{LJ}$, two orders of magnitude longer than $1/\dot{\gamma}$; this time is sufficient to equilibrate the longitudinal modes under the constraint of overall stretching, thus allowing tension blobs to generate elastic entropic force, as we assumed in the shear slit model. The sharp drop of all autocorrelation functions at longer times is due to tumbling. In the y and z directions, the situation is very different, with relaxation occurring even somewhat faster than in equilibrium; more specifically, the autocorrelation function for the z direction is the closest to equilibrium, especially at $k > g_s$, while in the y direction, it decays even faster.

These observations support our shear slit model, invite generalizations, and generate several interesting open questions.

Generalizations and Open Questions. Our results should be applicable to other self-similar polymer systems.

The easiest example is that of unentangled melts of linear polymers. For these, our naive theory, either in terms of shear blobs or the Cox−Merz rule, predicts $\eta = \eta_0(\dot{\gamma}\tau_{relax})^{-1/2}$ for $\dot{\gamma}\tau_{relax} > 1$, where in this case, $\tau_{relax} \approx \tau_0 N^2$ is the Rouse relaxation time. Experiments[45] have shown $\alpha = 1/2$ for unentangled polymer melts, in agreement with the predictions of the shear blob model and the Cox−Merz rule. Non-equilibrium molecular dynamics (NEMD) simulations[72,73] have been performed to study the nonlinear shear rheology of unentangled linear polymers. Barsky and Robbins[72] observed $\eta(\dot{\gamma}) \sim \dot{\gamma}^{-0.47}$ in their simulations based on the generic bead-spring model. The shear slit model predicts violation of universality, with viscosity decreasing faster than $(\dot{\gamma}\tau_{relax})^{-1/2}$ and nonmonotonically dependent on the chain length N.

Entangled linear chains at a very high shear rate $\dot{\gamma} > 1/\tau_e$ should look and behave similar to rings, as Figure 12A indicates.

We further predict that a similar argument should also be applicable to other self-similar polymer systems, such as, e.g., polymers close to the gelation point, but the details of this prediction are subject of a separate publication.

Of course, the overall picture that we presented is no more than a sketch. Although our main finding of two relevant scales for the rings in the shear flow and the nested set of tension and shear blobs, associated with velocity and velocity gradient directions, respectively, and directly related to the two normal stress differences (see eq 12), seems well justified, several aspects of the problem remain unclear. First and foremost, what is the mechanism confining every ring within a shear slit? We hypothesize the existence of some sort of a self-consistent potential, arising presumably from the dynamics of sheared neighboring chains with their steric interactions and perhaps with some (probably decreasing with an increasing shear rate) role of inter- and intrachain topological constraints. This self-consistent potential suppresses chain fluctuations in the y direction beyond the shear blob scale ξ_s; the idea is that on larger length/time scales, the chain sections attempting to leave the self-consistent slit by fluctuations are advected by the flow back into the layer. How to understand this potential quantitatively and eventually how to compute it from microscopic theory are an interesting challenge. Closely related is the question to what extent the shear slit is tilted; we show it somewhat tilted in Figure 1, but we do not know exactly the angle. Our preliminary data suggest that the distribution of eigenvalues λ_i of the inertia tensor is significantly skewed, suggesting the necessity to look at the joint distributions of eigenvalues and orientations of eigenvectors. The next open question is about the fractal structure of the chain inside the shear slit. We assumed, based on our computational data (see specifically Figure 14) that chains retain compact fractal globule statistics in the y direction ($y_k \sim k^{1/3}$) despite the fact that stretching in the x direction could be thought to ease topological constraints. A deeper understanding of this issue is desirable. As we pointed out, stretching of the chain by the shear flow is not uniform; it is maximal in the middle between the largest and smallest x ends for every chain and gradually diminishes closer to these ends. That means, tension blobs are only roughly the same size everywhere, and it is necessary to address the resulting "trumpet"-like behavior.

One of the avenues to address these questions may be related to our predictions regarding normal stress differences and their relation to viscosity, see eqs 12 and 13 and accompanying comments. To pursue this further, one has to realize that eqs 12 and 13 are written for the system in a nonlinear regime, when $Wi > 1$, and accordingly, shear and tension blobs are significantly shorter than the chain, $g_t < g_s < N/2$. In the linear regime, at $Wi < 1$, each ring is only weakly compressed in the direction of the velocity gradient (y) and only weakly stretched in the velocity direction (x), yielding a smooth dependence of normal stresses on the shear rate, which can be established based on linear response theory and our knowledge of the equilibrium fractal globule state of rings in the melt (e.g., ref 9).

The next group of open questions has to do with chain dynamics, including the nature of tumbling. In our simulations, we observe time between tumbling episodes longer than $1/\dot{\gamma}$. Why is it so long, and how can we estimate it as well as the duration of one tumbling event? This renders further investigations by simulations and experiments necessary. Tumbling is also important to understand the dramatic difference between shear thinning considered here and strong thickening observed for rings in an extensional flow (see ref 29) and in certain active systems (ref 70), where two or more rings can topologically connect in a so-called cow hitch knots. In both extensional flow and active systems, this happens because although the formation rate of cow hitch knot configuration is not high, the rate of its undoing is exceedingly

small because either the flow or the activity keeps the knot very tight all the time, producing a very high barrier for untying. By contrast, in a shear flow, tumbling episodes relax tensions, and thus, cow hitch knots are practically never seen.

Our main results were about universal (at moderate shear rates, where nonconcatenated ring polymers exhibit aspects of topology-induced double folding and crumpling but are not yet stretched on the Kuhn scale) and nonuniversal (at very large shear rates, when chains are stretched on the Kuhn scale) regimes of viscosity. A more thorough investigation of universality will be needed to incorporate aspects such as the number of entanglements per one Kuhn segment or friction reduction, when Kuhn segments align with the flow (see, in particular, ref 74). One of the inviting possibilities in this direction is to simulate Kremer–Grest models with a range of flexibilities, starting from the fully flexible one, which, according to the recent work,[75] may more accurately map on the experimental PS data.

In the present paper, we mostly addressed the shear thinning and normal stress difference, while other phenomena in nonlinear rheology are not less interesting, such as, e.g., stress overshoot and undershoot. We hope that the theoretical ideas developed here may prove useful for this purpose in combination with simulations and experiments.

Future theory will have to answer these and several other serious questions in order to understand the situation more fully. We leave them as a challenge for the future.

■ CONCLUSIONS

In this work, we have presented a systematic investigation of the steady-state shear viscosity of entangled unconcatenated ring polymers. For this, we combined experiments, simulations, and theoretical modeling. We used two experimentally pure ring polystyrenes with molar masses of 84 and 185 kg/mol, which correspond to about $Z = 5$ and $Z = 11$ entanglements, and compared them with their linear precursors. Obtaining pure unconcatenated ring polymers remains a challenge; although up to $Z = 44$ has been reported,[6] $Z = 11$ is the largest examined so far in terms of nonlinear rheology. We overcome this limitation using nonequilibrium MD simulations, which we were able to extend to $Z = 57$. We found that entangled rings exhibit much weaker shear thinning compared to their linear counterparts. The experimental power law thinning exponent (eq 1) for rings is 0.56 ± 0.02, that from simulations is 0.57 ± 0.08, and from theory is 0.57, all mutually consistent. The respective values for linear polymers are 0.89 ± 0.05 (experiments) and 0.80 ± 0.06 (simulations). The value of the shear thinning exponent can be explained by a naive scaling theory making an ad hoc assumption that viscosity is dominated by the dynamical modes in the velocity gradient direction with th elength and time scale up to a shear blob, i.e., a chain section with relaxation time $1/\dot{\gamma}$ (smaller than the relaxation time of the ring). We justified the above assumption by developing a shear slit model involving not one but two distinct length scales, that of shear blobs in the gradient direction and a smaller one of tension blobs in the velocity direction. This nested system of blobs and associated normal stress differences form because dynamic modes of the chain in different directions behave very differently. Specifically, in the time between subsequent tumbling episodes, longitudinal modes along the flow direction (or at least a significant fraction of them) have time to equilibrate, subject to the constraint of strong stretching, but these modes do not contribute to viscosity, which is controlled by modes in the velocity gradient direction (those of them faster than $1/\dot{\gamma}$). At the same time, modes in the direction of the velocity gradient are self-consistently constrained to within the scale of shear blobs; these modes dissipate, while longer wavelength modes are uncoupled and do not contribute to viscosity. In this sense, viscosity of melts of sheared rings is similar to linear viscosity of unconnected sections of rings of the size about shear slit width.

■ ASSOCIATED CONTENT

ⓈI Supporting Information

The Supporting Information is available free of charge at https://pubs.acs.org/doi/10.1021/acs.macromol.0c02839.

Tables of experimental and simulation data, tables of theoretical formulas for various scaling regimes, interpolation expressions for relaxation moduli of linear chains and rings, and detailed analysis of the Cox–Merz rule in various forms (PDF)

■ AUTHOR INFORMATION

Corresponding Authors

Dimitris Vlassopoulos − *FORTH and University of Crete, Heraklion 71110, Greece;* ⊙ orcid.org/0000-0003-0866-1930; Email: dvlasso@iesl.forth.gr

Michael Rubinstein − *Duke University, Durham, North Carolina 27708-9976, United States; Hokkaido University, Sapporo, Hokkaido 060-0808, Japan;* ⊙ orcid.org/0000-0002-5455-0951; Email: michael.rubinstein@duke.edu

Alexander Y. Grosberg − *New York University, New York 10003, United States;* ⊙ orcid.org/0000-0002-4230-8690; Email: ayg1@nyu.edu

Authors

Daniele Parisi − *FORTH and University of Crete, Heraklion 71110, Greece; Penn State University, State College, Pennsylvania 16801, United States*

Salvatore Costanzo − *FORTH and University of Crete, Heraklion 71110, Greece; University of Naples Federico II, Naples 80125, Italy;* ⊙ orcid.org/0000-0003-1780-389X

Youncheol Jeong − *Pohang University of Science and Technology, Pohang 790-784, South Korea*

Junyoung Ahn − *Pohang University of Science and Technology, Pohang 790-784, South Korea*

Taihyun Chang − *Pohang University of Science and Technology, Pohang 790-784, South Korea;* ⊙ orcid.org/0000-0003-2623-1803

Jonathan D. Halverson − *Princeton University, Princeton, New Jersey 08544, United States*

Kurt Kremer − *Max Planck Institute for Polymer Research, Mainz 55021, Germany;* ⊙ orcid.org/0000-0003-1842-9369

Ting Ge − *University of South Carolina, Columbia, South Carolina 29208-0001, United States;* ⊙ orcid.org/0000-0003-2456-732X

Gary S. Grest − *Sandia National Laboratories, Albuquerque, New Mexico 87185, United States;* ⊙ orcid.org/0000-0002-5260-9788

Watee Srinin − *Naresuan University, Mueang Phitsanulok, Phitsanulok 65000, Thailand*

Complete contact information is available at:
https://pubs.acs.org/10.1021/acs.macromol.0c02839

ADDITIONAL NOTES

[1] Formula eq 1 is a particular case of the so-called Carreau–Yasuda equation $\eta(\dot{\gamma}) = \eta_\infty + (\eta_0 - \eta_\infty)[1 + (\dot{\gamma}\tau_{relax})^a]^{(n-1)/a}$ (see refs 21–23 or a textbook[24]). For our purposes, it is sufficient to use the simplified version (eq 1), with $\eta_\infty = 0$, $n - 1 \rightarrow -\alpha$, and $a = 1$. The other frequently used simple version (see, e.g., the Doi book[25]), with $\eta_\infty = 0$, $n - 1 \rightarrow -\alpha$, and $a = \alpha$, does not fit our data very well.

[2] We shall stick to the traditional though admittedly loose terminology of the "velocity gradient" direction; in fact, velocity as a vector cannot have a gradient, and what is really meant is the direction perpendicular to both velocity and vorticity, i.e. $\mathbf{v} \times (\nabla \times \mathbf{v}) \equiv \nabla(\mathbf{v}^2)$.

[3] We here do not touch upon various ways to estimate the onset of the entangled regime for either the rings or the linear chains, which produce results related to the above defined N_e but different depending on both the specific quantity measured and on chain architecture. We also do not discuss the possibility to bypass the true dynamics measurement in order to determine N_e by performing the so-called primitive path analysis.[46,47]

[4] Complex viscosity is defined by any of the following equivalent representations: $\eta^*(\omega) = G^*(\omega)/i\omega = G''(\omega)/\omega - iG'(\omega)/\omega = \int_0^\infty G(t)e^{i\omega t}dt$.

[5] It is interesting to note that the relation $\langle x_{N/2}^2 \rangle = 4\lambda_1$ holds, with a similar accuracy, also for other tested values of the shear rate, $\dot{\gamma}\tau_{LJ} = 10^{-3}$ ($\lambda_1 \approx 5000\sigma^2$, $\langle x_{N/2}^2 \rangle \approx 20,000$) and 10^{-2} ($\lambda_1 \approx 6500\sigma^2$, $\langle x_{N/2}^2 \rangle \approx 28,000$), lending additional support for the idea of a loop stretched along a line.

REFERENCES

(1) Doi, M.; Edwards, S. F. *The Theory of Polymer Dynamics*; Clanderon Press: Oxford, 1986.

(2) Rubinstein, M.; Colby, R. H. *Polymer Physics*; Oxford University Press: 2003.

(3) De Gennes, P. G. Reptation of stars. *J. Phys. France* **1975**, *36*, 1199–1203.

(4) McLeish, T. Polymer dynamics: Floored by the rings. *Nat. Mater.* **2009**, *7*, 933–935.

(5) Halverson, J. D.; Lee, W. B.; Grest, G. S.; Grosberg, A. Y.; Kremer, K. Molecular Dynamics Simulation Study of Nonconcatenated Ring Polymers in a Melt: I. Statics. *J. Chem. Phys.* **2011**, *134*, 204904.

(6) Kruteva, M.; Allgaier, J.; Monkenbusch, M.; Porcar, L.; Richter, D. Self-Similar Polymer Ring Conformations Based on Elementary Loops: A Direct Observation by SANS. *ACS Macro Lett.* **2020**, *9*, 507–511.

(7) Kapnistos, M.; Lang, M.; Vlassopoulos, D.; Pyckhout-Hintzen, W.; Richter, D.; Cho, D.; Chang, T.; Rubinstein, M. Unexpected power-law stress relaxation of entangled ring polymers. *Nat. Mater.* **2008**, *7*, 997–1002.

(8) Smrek, J.; Grosberg, A. Y. Understanding the dynamics of rings in the melt in terms of the annealed tree model. *J. Phys.: Condens. Matter* **2015**, *27*, No. 064117.

(9) Ge, T.; Panyukov, S.; Rubinstein, M. Self-Similar Conformations and Dynamics in Entangled Melts and Solutions of Nonconcatenated Ring Polymers. *Macromolecules* **2016**, *49*, 708–722.

(10) Halverson, J. D.; Lee, W. B.; Grest, G. S.; Grosberg, A. Y.; Kremer, K. Molecular Dynamics Simulation Study of Nonconcatenated Ring Polymers in a Melt: II. Dynamics. *J. Chem. Phys.* **2011**, *134*, 204905.

(11) Michieletto, D.; Marenduzzo, D.; Orlandini, E.; Turner, M. Ring Polymers: Threadings, Knot Electrophoresis and Topological Glasses. *Polymer* **2017**, *9*, 349–369.

(12) Smrek, J.; Kremer, K.; Rosa, A. Threading of Unconcatenated Ring Polymers at High Concentrations: Double-Folded vs Time-Equilibrated Structures. *ACS Macro Lett.* **2019**, *8*, 155–160.

(13) Arrighi, V.; Higgins, J. S. Local Effects of Ring Topology Observed in Polymer Conformation and Dynamics by Neutron Scattering—A Review. *Polymer* **2020**, *12*, 1884.

(14) Ahmadian Dehaghani, Z.; Chubak, I.; Likos, C. N.; Ejtehadi, M. R. Effects of topological constraints on linked ring polymers in solvents of varying quality. *Soft Matter* **2020**, *16*, 3029–3038.

(15) Rauscher, P. M.; Schweizer, K. S.; Rowan, S. J.; de Pablo, J. J. Thermodynamics and Structure of Poly[n]catenane Melts. *Macromolecules* **2020**, *53*, 3390–3408.

(16) Klotz, A. R.; Soh, B. W.; Doyle, P. S. Equilibrium Structure and Deformation Response of 2D Kinetoplast Sheets. *Proc. Nat. Acad. Sci. U. S. A.* **2020**, *117*, 121–127.

(17) Liebetreu, M.; Likos, C. N. Shear-Induced Stack Orientation and Breakup in Cluster Glasses of Ring Polymers. *ACS Appl. Polym. Mater.* **2020**, *2*, 3505–3517.

(18) Landuzzi, F.; Nakamura, T.; Michieletto, D.; Sakaue, T. Persistence Homology of Entangled Rings. *Phys. Rev. Res.* **2020**, *2*, No. 033529.

(19) Pachong, S. M.; Chubak, I.; Kremer, K.; Smrek, J. Melts of nonconcatenated rings in spherical confinement. *J. Chem. Phys.* **2020**, *153*, No. 064903.

(20) Wang, S.-Q. *Nonlinear Polymer Rheology: Macroscopic Phenomenology and Molecular Foundation*; Wiley: (Hoboken, NJ), 2018.

(21) Carreau, P. J. Rheological equations from molecular network theories. *J. Rheol.* **1972**, *16*, 99–127.

(22) Yasuda, K. *Investigation of the analogies between viscometric and linear viscoelastic properties of polystyrene fluids (579 pages)*. Ph.D. thesis, MIT, 1979; URL: https://dspace.mit.edu/handle/1721.1/16043.

(23) Yasuda, K.; Armstrong, R. C.; Cohen, R. E. Shear flow properties of concentrated solutions of linear and star branched polystyrenes. *Rheol. Acta* **1981**, *20*, 163–178.

(24) Dealy, J. M.; Wang, J. *Melt rheology and its applications in the plastics industry*; 2nd ed.; Springer: 2013, DOI: 10.1007/978-94-007-6395-1.

(25) Doi, M. *Soft Matter Physics*; Clanderon Press: Oxford, 2013

(26) Huang, Q.; Ahn, J.; Parisi, D.; Chang, T.; Hassager, O.; Panyukov, S.; Rubinstein, M.; Vlassopoulos, D. Unexpected Stretching of Entangled Ring Macromolecules. *Phys. Rev. Lett.* **2019**, *122*, 208001.

(27) Yan, Z. C.; Costanzo, S.; Jeong, Y.; Chang, T.; Vlassopoulos, D. Linear and Nonlinear Shear Rheology of a Marginally Entangled Ring Polymer. *Macromolecules* **2016**, *49*, 1444−1453.

(28) Yoon, J.; Kim, J.; Baig, C. Nonequilibrium Molecular Dynamics Study of Ring Polymer Melts under Shear and Elongation Flows: A Comparison with their Linear Analogs. *J. Rheol.* **2016**, *60*, 673−685.

(29) O'Connor, T. C.; Ge, T.; Rubinstein, M.; Grest, G. S. Topological Linking Drives Anomalous Thickening of Ring Polymers in Weak Extensional Flows. *Phys. Rev. Lett.* **2020**, *124*, No. 027801.

(30) Halverson, J. D.; Grest, G. S.; Grosberg, A. Y.; Kremer, K. Rheology of Ring Polymer Melts: From Linear Contaminants to Ring-Linear Blends. *Phys. Rev. Lett.* **2012**, *108*, No. 038301.

(31) Jeong, S.; Cho, S.; Kim, J. M.; Baig, C. Interfacial Molecular Structure and Dynamics of Confined Ring Polymer Melts under Shear Flow. *Macromolecules* **2018**, *51*, 4670−4677.

(32) Tsamopoulos, A. J.; Katsarou, A. F.; Tsalikis, D. G.; Mavrantzas, V. G. Shear Rheology of Unentangled and Marginally Entangled Ring Polymer Melts from Large-Scale Nonequilibrium Molecular Dynamics Simulations. *Polymer* **2019**, *11*, 1194.

(33) Carl, W. Configurational and rheological properties of cyclic polymers. *Faraday Trans.* **1995**, *91*, 2525−2530.

(34) Cifre, J. G. H.; Pamies, R.; Martnez, M. C. L.; de la Torre, J. G. Steady-state Behavior of Ring Polymers in Dilute Flowing Solutions via Brownian Dynamics. *Polymer* **2005**, *46*, 267−274.

(35) Chen, W.; Li, Y.; Zhao, H.; Liu, L.; Chen, J.; An, L. Conformations and dynamics of single flexible ring polymers in simple shear flow. *Polymer* **2015**, *64*, 93−99.

(36) Chen, W.; Chen, J.; An, L. Tumbling and Tank-treading Dynamics of Individual Ring Polymers in Shear Flow. *Soft Matter* **2013**, *9*, 4312−4318.

(37) Cox, W. P.; Merz, E. H. Correlation of dynamic and steady flow viscosities. *Journal of Polymer Science* **1958**, *28*, 619.

(38) Rabin, Y.; Öttinger, H. C. Dilute Polymer Solutions: Internal Viscosity, Dynamic Scaling, Shear Thinning and Frequency-Dependent Viscosity. *Europhys. Lett.* **1990**, *13*, 423−428.

(39) Teixeira, R. E.; Babcock, H. P.; Shaqfeh, E. S. G.; Chu, S. Shear Thinning and Tumbling Dynamics of Single Polymers in the Flow-Gradient Plane. *Macromolecules* **2005**, *38*, 581−592.

(40) Aoyagi, T.; Doi, M. Molecular dynamics simulation of entangled polymers in shear flow. *Comput. Theor. Polym. Sci.* **2000**, *10*, 317−321.

(41) Baig, C.; Mavrantzas, V. G.; Kröger, M. Flow effects on melt structure and entanglement network of linear polymers: Results from a nonequilibrium molecular dynamics simulation study of a polyethylene melt in steady shear. *Macromolecules* **2010**, *43*, 6886−6902.

(42) Kim, J. M.; Edwards, B. J.; Keffer, D. J.; Khomami, B. Dynamics of individual molecules of linear polyethylene liquids under shear: Atomistic simulation and comparison with a free-draining bead-rod chain. *J. Rheol.* **2010**, *54*, 283−310.

(43) Dambal, A.; Kushwaha, A.; Shaqfeh, E. S. G. Slip-link simulations of entangled, finitely extensible, wormlike chains in shear flow. *Macromolecules* **2009**, *42*, 7168−7183.

(44) Sefiddashti, M. H. N.; Edwards, B. J.; Khomami, B. Individual chain dynamics of a polyethylene melt undergoing steady shear flow. *J. Rheol.* **2015**, *59*, 119−153.

(45) Colby, R. H.; Boris, D. C.; Krause, W. E.; Dou, S. Shear thinning of unentangled flexible polymer liquids. *Rheol. Acta* **2007**, *46*, 569−575.

(46) Everaers, R.; Sukumaran, S. K.; Grest, G. S.; Svaneborg, C.; Sivasubramanian, A.; Kremer, K. Rheology and Microscopic Topology of Entangled Polymeric Liquids. *Science* **2004**, *303*, 823−826.

(47) Hsu, H.-P.; Kremer, K. Static and dynamic properties of large polymer melts in equilibrium. *J. Chem. Phys.* **2016**, *144*, 154907.

(48) Ziebarth, J. D.; Gardiner, A. A.; Wang, Y.; Jeong, Y.; Ahn, J.; Jin, Y.; Chang, T. Comparison of Critical Adsorption Points of Ring Polymers with Linear Polymers. *Macromolecules* **2016**, *49*, 8780−8788.

(49) Jeong, Y.; Jin, Y.; Chang, T.; Uhlik, F.; Roovers, J. Intrinsic Viscosity of Cyclic Polystyrene. *Macromolecules* **2017**, *50*, 7770−7776.

(50) Costanzo, S.; Huang, Q.; Ianniruberto, G.; Marrucci, G.; Hassager, O.; Vlassopoulos, D. Shear and Extensional Rheology of Polystyrene Melts and Solutions with the Same Number of Entanglements. *Macromolecules* **2016**, *49*, 3925−3935.

(51) Costanzo, S.; Ianniruberto, G.; Marrucci, G.; Vlassopoulos, D. Measuring and assessing first and second normal stress differences of polymeric fluids with a modular cone-partitioned plate geometry. *Rheol. Acta* **2018**, *57*, 363−376.

(52) Ferry, J. D. *Viscoelastic properties of polymers*; 3rd ed.; Wiley; 1980.

(53) Walsh, D.; Zoller, P. *Standard Pressure Volume Temperature Data for Polymers*; CRC Press, 1995.

(54) Dealy, J. M. Weissenberg and Deborah Numbers - Their Definition and Use. *Rheol. Bull.* **2010**, *79*, 14−18.

(55) Kremer, K.; Grest, G. S. Dynamics of entangled linear polymer melts: A molecular-dynamics simulation. *J. Chem. Phys.* **1990**, *92*, 5057.

(56) Evans, D. J.; Morriss, G. P. Nonlinear-response theory for steady planar Couette flow. *Phys. Rev. A* **1984**, *30*, 1528.

(57) Daivis, P. J.; Todd, B. D. A simple, direct derivation and proof of the validity of the SLLOD equations of motion for generalized homogeneous flows. *J. Chem. Phys.* **2006**, *124*, 194103.

(58) Evans, D. J.; Morriss, G. P. *Statistical Mechanics of Non-equilibrium Liquids*; Elsevier: (Amsterdam), 1990.

(59) Kröger, M.; Loose, W.; Hess, S. Rheology and structural changes of polymer melts via nonequilibrium molecular dynamics. *J. Rheol.* **1993**, *37*, 1057.

(60) Kröger, M.; Hess, S. Rheological Evidence for a Dynamical Crossover in Polymer Melts via Nonequilibrium Molecular Dynamics. *Phys. Rev. Lett.* **2000**, *85*, 1128−1131.

(61) Cao, J.; Likhtman, A. E. Simulating Startup Shear of Entangled Polymer Melts. *ACS Macro Lett.* **2015**, *4*, 1376−1381.

(62) Moreira, L. A.; Zhang, G.; Müller, F.; Stuehn, T.; Kremer, K. Direct Equilibration and Characterization of Polymer Melts for Computer Simulations. *Macromol. Theory Simul.* **2015**, *24*, 419−431.

(63) Pasquino, R.; et al. Viscosity of Ring Polymer Melts. *ACS Macro Lett.* **2013**, *2*, 874−878.

(64) Gooßen, S.; Brás, A. R.; Krutyeva, M.; Sharp, M.; Falus, P.; Feoktystov, A.; Gasser, U.; Pyckhout-Hintzen, W.; Wischnewski, A.; Richter, D. Molecular Scale Dynamics of Large Ring Polymers. *Phys. Rev. Lett.* **2014**, *113*, 168302.

(65) Rosa, A.; Everaers, R. Ring Polymers in the Melt State: The Physics of Crumpling. *Phys. Rev. Lett.* **2014**, *112*, 118302.

(66) Michieletto, D.; Turner, M. S. A topologically driven glass in ring polymers. *Proc. Natl. Acad. Sci. U. S. A.* **2016**, *113*, 5195−5200.

(67) Tsalikis, D. G.; Mavrantzas, V. G.; Vlassopoulos, D. Analysis of Slow Modes in Ring Polymers: Threading of Rings Controls Long-Time Relaxation. *ACS Macro Lett.* **2016**, *5*, 755−760.

(68) Kruteva, M.; Allgaier, J.; Richter, D. Direct Observation of Two Distinct Diffusive Modes for Polymer Rings in Linear Polymer Matrices by Pulsed Field Gradient (PFG) NMR. *Macromolecules* **2017**, *50*, 9482−9493.

(69) Doi, Y.; Matsubara, K.; Ohta, Y.; Nakano, T.; Kawaguchi, D.; Takahashi, Y.; Takano, A.; Matsushita, Y. Melt rheology of ring polystyrenes with ultrahigh purity. *Macromolecules* **2015**, *48*, 3140−3147.

(70) Smrek, J.; Chubak, I.; Likos, C. N.; Kremer, K. Active topological glass. *Nat. Commun.* **2020**, *11*, 26−36.

(71) Larson, R. G. *The Structure and Rheology of Complex Fluids*; Oxford University Press: 1999.

(72) Barsky, S.; Robbins, M. O. Bulk and interfacial shear thinning of immiscible polymers. *Phys. Rev. E* **2002**, *65*, No. 021808.

(73) Moore, J. D.; Cui, S. T.; Cochran, H. D.; Cummings, P. T. A molecular dynamics study of a short-chain polyethylene melt. *J. Non-Newtonian Fluid Mech.* **2000**, *93*, 83−99.

(74) Wingstrand, S. L.; Alvarez, N. J.; Huang, Q.; Hassager, O. Linear and Nonlinear Universality in the Rheology of Polymer Melts and Solutions. *Phys. Rev. Lett.* **2015**, *115*, No. 078302.

(75) Everaers, R.; Karimi-Varzaneh, H. A.; Fleck, F.; Hojdis, N.; Svaneborg, C. Kremer-Grest Models for Commodity Polymer Melts: Linking Theory, Experiment, and Simulation at the Kuhn Scale. *Macromolecules* **2020**, *53*, 1901−1916.